

# Chapter 7

## Higher-Order Modulation Formats – Concepts and Enabling Devices

Wilfried Idler and Fred Buchali

**Abstract** The chapter gives a general introduction to higher-order modulation (HOM) formats and reviews the current status of concepts of coherent transceivers applied in optical fiber communications. The chapter presents an overview on the major enablers of HOM formats in optical transmission: forward error correction, digital signal processing, data converter, DP-IQ modulator, receiver frontend and application-specific integrated circuit (ASIC) technology. Based on the examples of current and future 400 Gbit/s and 1 Tbit/s transceivers the chapter illustrates feasible transmission capacities and transmission reach with HOM formats based on EDFA repeated C-band transmission over dispersion uncompensated standard single mode fiber.

### 7.1 Introduction

Over the past 20 years the worldwide Internet traffic has grown exponentially and cumulated annual growth rates (CAGRs) have been of the order of 100% during the period from 1995 to 2000, and even after the “burst of the bubble” impressive ~40% CAGRs have been achieved up to 2013, primarily driven by data-centric users. This growth in traffic has been enabled by tremendous increments of transport capacity of the fiber optical networks, and this development is still going on. Latest forecasts in 2016 [1] predict that until 2020 the global Internet traffic will still continue to grow worldwide with a CAGR of about 22%.

Figure 7.1 shows the progress and status of single fiber capacities on the optical C-band and transmission bit rate achievements in research and product implementations from 1988 until 2014, and Fig. 7.1 also illustrates a CAGR trend of 22% (grey arrow) for the fiber capacity utilization between 2014 and 2020.

In DWDM fiber networks the capacity of a single fiber has been increased from 1 Gbit/s with a single carrier modulated with 1 Gbit/s NRZ in the mid-1980s to al-

---

W. Idler (✉) · F. Buchali  
Nokia Bell Labs, Lorenzstraße 10, 70435 Stuttgart, Germany  
e-mail: [wilfried.idler@nokia-bell-labs.com](mailto:wilfried.idler@nokia-bell-labs.com)

F. Buchali  
e-mail: [fred.buchali@nokia-bell-labs.com](mailto:fred.buchali@nokia-bell-labs.com)

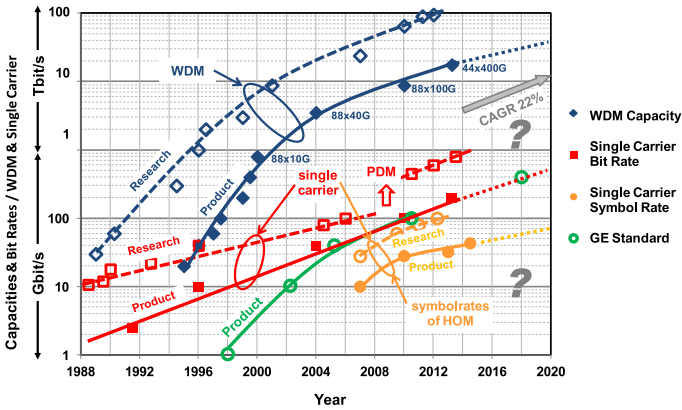


**Fig. 7.1** C-band fiber capacities and increase of bit rates over the years in research and products

most 1 Tbit/s by 2000. Based upon progress in TDM technology single carrier bit rates have been raised from 1 Gbit/s to 2.5 Gbit/s and 10 Gbit/s NRZ, and in combination with the introduction of WDM technology in 1995 [2], five years later in 2000, 880 Gbit/s total capacity was achieved on a single fiber with 10 Gbit/s  $\times$  88 channels in the C-band on the 50 GHz standard grid. Determined by the optical bandwidth of EDFA repeaters we are considering throughout this chapter 4.4 THz optical bandwidth ( $\sim$ 35 nm) for the C-band and the supported single fiber capacities.

In order to further increase the capacity from 10 Gbit/s towards the next transport hierarchy of 40 Gbit/s, research has focused on modulation formats other than NRZ which spectrally fit into the 50 GHz grid. First 40 Gbit/s WDM products started in 2004 and were based on optical duobinary (ODB) and differential quaternary phase shift keying (DQPSK) for Metro applications with direct detection receivers. They achieved spectral efficiencies (SE) of 0.8 bit/s/Hz and enabled up to 3.5 Tbit/s fiber transport capacity in 2004. DQPSK was the first product implementation in optical transport with a multi-level higher order modulation (HOM) format, modulating 4 phase levels. Six years earlier a multi-level format on the basis of 4 amplitude modulated levels (4ASK), also denoted as 4PAM (pulse amplitude modulation), had been proposed in research as an early solution for 40 Gbit/s bit rates [3] based on 20 GBd symbol rate electronics. Recently the 4PAM format became of high interest for 400 Gigabit Ethernet (GE) transport [4]. All 40 Gbit/s direct detection Metro and long haul transport systems have been challenged with fiber polarization mode dispersion (PMD) as well as the need for a further increase of the SE by including polarization division multiplexing (PDM). A major breakthrough of reaching SE beyond 1 bit/s/Hz and the mitigation of issues related to PMD and PDM has been achieved after 2008 with coherent receiver technology and the implementation of 100 Gbit/s systems based on PDM or dual-polarization (DP) and QPSK modulation formats in 2010. The key of the rediscovery of coherent receiver technology and the key enabler for the effective use of HOMs were the introduction of analogue-to-digital data

converters (ADCs) and digital signal processing (DSP) in optical communication enabled by the continuous progress of complementary metal-oxide semiconductor (CMOS) technology.

In recent years complex HOM formats based on quadrature amplitude modulation (QAM) became indispensable in all digital communication areas in order to increase transmission bit rates over existing infrastructures by increasing spectral efficiency and capacity [5]. In telephone modems or at cable based digital video broadcast (DVB-C2) very high constellation sizes of 4096QAM are applied. However, in optical communication the transmission bit rates are significantly higher and signal-to-noise-ratio values at optical receivers are significantly lower, and therefore constellation sizes applicable for optical communication products are significantly lower. Nevertheless, constellation sizes as high as 1024QAM [6] and even 2048QAM [7] have been demonstrated in optical communication research, requiring very narrow linewidth lasers and Raman amplification for transmission demonstration.

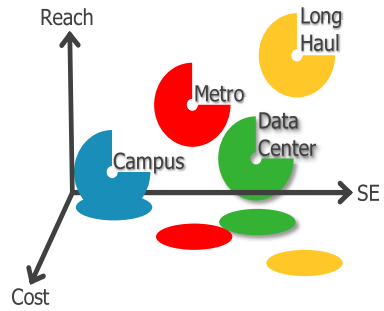
100 Gbit/s based on DP-QPSK with coherent detection became a preferred solution [8] as it can be applied on existing 50 GHz grid fiber infrastructure, operating with 28 GBd symbol rate. QPSK is encoding two bits/symbol and together with PDM four bits are encoded on each symbol. Since the first commercial deployment of 100 Gbit/s line cards with DP-QPSK on a single carrier in 2010, about 300,000 line cards [9] have already been deployed until mid 2016. According to [10], until 2020 the demand for 100 Gbit/s (and higher) line cards will grow with a CAGR of about 120%. On the other hand, 40 Gbit/s line card deployments are continuously dropping, they became less than 10% of 100 Gbit/s line card shipments in 2016 [9], as many operators apparently move from 10 Gbit/s directly to 100 Gbit/s systems.

The most recent bit rate hierarchy started in 2014 with 400 Gbit/s systems based on 200 Gbit/s and the DP-16QAM HOM format with an SE of 4 bit/s/Hz. Including frequency division multiplexing (FDM) by combining two sub-carriers,  $2 \times 200$  Gbit/s can also be transported over the 50 GHz grid capturing two frequency slots of 50 GHz. Thus the C-band capacity of a single fiber with 4.4 THz bandwidth reaches  $\sim 18$  Tbit/s.

The use of HOM formats together with orthogonal frequency division multiplexing (OFDM) has been intensively investigated for optical transmission applications. OFDM is somewhat less spectrally efficient than the corresponding single carrier schemes can be when they are modulated with the same HOM formats, due to cyclic prefix, pilot, and training symbol overhead requirements [11]. Furthermore, as OFDM uses a rather high number of sub-carriers and low symbol rates, OFDM is severely impaired by inter-channel and intra-channel fiber non-linear effects, especially at dispersion managed transmission. The latter is dominated by strong self-phase modulation (SPM) due to the narrow spectral width of the individually modulated carriers as SPM tolerance is increasing with the symbol rate [12]. This is one reason why OFDM systems have not yet been deployed and will not be considered further in this chapter.

Recently, HOM formats together with discrete multitone transmission (DMT) using directly modulated lasers and direct detection have been proposed as a low cost alternative for 100 Gbit/s [13] and for 400 Gbit/s [14] short reach transmission (see

**Fig. 7.2** Applications triangle



also Chap. 4, Sect. 4.5.2). DSP in direct detection DMT is comparable with OFDM but DMT rejects the complex part of the received signal. However, even if a high constellation size such as 128QAM [13] is applied, DMT is not spectrally efficient for DWDM networks due to the poor frequency stability of directly modulated and uncooled DFB lasers, and therefore the proposed application area of DMT is short reach CWDM [15] with 20 nm channel spacing. Similar to OFDM, DMT does also apply a very high number of sub-carriers ( $> 1000$ ) and symbol rates per sub-carrier in the few Mbd regime. Therefore DMT does also suffer from SPM so that its application space is limited to short reach or intra campus applications. As OFDM, DMT will also not be treated in this chapter.

The application areas of optical transmission systems have different requirements on capacity (spectral efficiency), the supported transmission distance (reach) and cost per transported bit, as depicted in Fig. 7.2. Application areas we will focus on in this chapter are intra data center, Metro and long haul. Connections between data centers (inter) are usually point-point long haul transmission links. Depending on country and continent the required distances for Metro and long haul are different but can roughly be separated: Metro below 500 km fiber distances and long haul between 500 km and 1000 km in Europe and up to 3000 km in North America. Intra data center distances are typically well below 50 km. Except for campus and access applications, for intra data center, Metro and long haul high spectral efficiencies are required but with different sensitivities to cost.

The application areas and corresponding capacity limits of HOM formats are determined by their OSNR (optical signal to noise ratio) constraints or sensitivities and the fiber infrastructure. Taking long haul fiber infrastructures for comparison, capacities can be increased by 150% by including L-band transmission [16], implementation of new fiber types with lower insertion loss and higher effective area [17], or including Raman amplification. Finally, depending on the development progress and future cost of regenerators, the use of high constellation sizes for 3R-regenerators could become very attractive for shifting the application boundaries of HOM formats towards higher constellation sizes.

If only widely deployed C-band transmission with standard single mode fibers (SMF) and EDFA repeaters are taken into account, the capacity limits per fiber of long haul networks in the order of 15 to 20 Tbit/s are reached with 8QAM and 16QAM, respectively. Metro network backbones supported by HOM formats can reach 35 Tbit/s with DP-64QAM, potentially implementable before 2020. Further

increments of the spectral efficiency and capacities up to 40 or 50 Tbit/s are feasible by 128QAM or 256QAM, but due to increasing OSNR constraints with increasing the constellation size of HOMs, regeneration for long haul transmission will be required or potential future application areas are limited to short reach, access and data centers.

SDM [18] has been proposed as the only way-out of potential future capacity bottlenecks for long haul and Metro networks and significant research has been performed in the past few years with amazing results (see also Chap. 1). Recently, very high spectral efficiencies above 300 bit/s/Hz [19] have already been demonstrated with transmission over a 19 core fiber where six modes appear coupled. Multiple-input and multiple-output (MIMO) DSP has become an essential element of wireless communication as a method for multiplying the capacity of a radio link using multiple transmit and receive antennas to exploit multipath propagation. In optical transmission research MIMO has been successfully demonstrated in multimode fiber transmission or in transmission of multi-core fibers where modes can also be coupled. The highest MIMO complexity has been reported with transmission over 15 coupled spatial modes in MMF by massive  $30 \times 30$  MIMO processing [20]. However, from today's perspective, the potential market maturity and implementation start of SDM are unknown as these are determined by many factors, mainly driven by future capacity requirements of operators' backbone and by the performance and cost of the new SDM technology.

A perpetual question is the degree of capacity utilization of operations backbone and when investments are needed for new technologies and higher fiber capacities. Today it appears very uncertain by what time single fiber capacities higher than 35 Tbit/s will be required and when SDM technologies will be needed or alternatively transmission including the optical L-band will be favored or regenerators for HOM formats become available or Raman amplification will be further pushed for implementation. Fiber utilization and capacity requirements vary significantly between applications, countries and operators, and neither analyst studies can provide reliable predictions of future developments. One often reported message is that 0.88 Tbit/s capacity per fiber is utilized and that operators had begun in 2014 already a capacity upgrade moving directly from 10G to 100G launching for a future completion of an 8.8 Tbit/s capacity. The arrow (CAGR 22%) in Fig. 7.1 indicates an optimistic case that with 3.6 Tbit/s capacity (e.g.:  $88 \times 40$  Gbit/s) already utilized in operators' Metro fiber backbone in 2014 and a 22% increase per year the capacity requirements will be  $\sim 10$  Tbit/s in 2020. Thus operators may not require single fiber capacities of 35 Tbit/s in earlier than 2020.

This chapter reviews the current status of concepts and enabling devices for HOM formats in optical transmission, comprised in current and future coherent transceivers: DP-MQAM formats are generated with transmitter DSP, digital-analogue converters (DACs) and IQ modulators and received with a coherent receiver frontend followed by ADCs and DSP. This chapter will be organized as follows: In Sect. 7.2 on optical transceivers we will highlight coherent receiver technology concepts and building blocks. In Sect. 7.3 we will focus on HOM formats suitable for three application areas (intra data center, Metro and long haul)

and analyze the transmission performance for the case without optical dispersion compensation and analyze achievable fiber transmission capacities versus application areas. In the following three sections we will present an overview on the key electronic concepts, the major enablers of HOM formats in optics: forward error correction (Sect. 7.4), digital signal processing (Sect. 7.5) and data converters (Sect. 7.6). Section 7.7 will focus on the enabling optical devices for HOM formats: DP-IQ modulator, receiver frontend and application-specific integrated circuit (ASIC) technology, including data converter and DSP, as the key components for the realization and implementation of QAM formats and reception for very high bit rate transmission.

## 7.2 Coherent Transceiver

### 7.2.1 *Reinvention of Coherent Receiver Technology*

In optical fiber communication, coherent receivers with free running local oscillator (LO) lasers, which exploit information in amplitude and phase, were extensively studied in the late eighties and early nineties of the last century [21–24]. This receiver concept was called “Intradyn Receiver” to be distinguished from a heterodyne receiver where the transmit laser frequency and the LO frequency can differ by more than the signal bandwidth.

Basically, we distinguish between three different coherent receiver concepts:

Homodyne: the optical signal spectrum is converted to the electrical baseband and a single common laser source is used for the transmitter (Tx) and as LO.

Intradyn: the optical signal spectrum is converted to the electrical baseband and two independent lasers for Tx and LO corresponding to the same channel number are applied but any frequency offset must be significantly smaller than the electrical baseband.

Heterodyne: the converted optical signal spectrum is converted outside the electrical baseband as the offset between Tx and LO lasers is larger than the signal bandwidth or the symbol rate.

Coherent detection of amplitude and phase is performed by mixing the modulated carrier signal with an LO into the baseband, a technique widely used in RF wireline and wireless telecommunication systems. The baseband signal is amplified by the LO and subsequently down-converted including appropriate filtering.

With the emergence of the EDFA in the early nineties of the last century, the advantage of higher receiver sensitivity of a coherent receiver compared to direct detection vanished and coherent receiver technology disappeared for more than 10 years. Since 2006 coherent optical systems are rediscovered as an area of very high interest again [25] and have revolutionized long haul and high-speed optical communication systems. Corresponding R&D activities were significantly pushed by Si hardware, in particular as high speed ADCs and electronic signal processors have become mature. In optical communications digital signal processing at the optical receiver has been commercialized at bit rates of 10 Gbit/s at first and coherent receivers at 40 Gbit/s later. Due to further progress in CMOS technologies until to-

day, data converters and DSP can now be realized by a single chip for 100 Gbit/s and 400 Gbit/s transceivers.

By coherent detection, all optical field parameters (amplitude, phase and polarization) become available in the electrical domain. Therefore the demodulation schemes are not limited to the detection of phase differences as for directly detected DPSK or DQPSK formats, but arbitrary modulation formats and modulation constellations including polarization multiplexed signals can be analyzed. The preservation of the temporal phase enables electronic compensation of linear transmission impairments such as chromatic dispersion [26, 27], and polarization mode dispersion (PMD), and even fiber nonlinearities can be partly mitigated at the electrical baseband. Many limitations and obstacles which existed in the past for the deployment of coherent detection have now been overcome: Carrier linewidth requirements become relaxed with increasing channel data and symbol rates so that standard commercial communication lasers can be used [28]. In addition, high-speed digital signal processing allows to perform fast polarization tracking, channel equalization, frequency and phase recovery, all processed in the electronic domain, which lifts the main barriers which have so far prevented to exploit the advantages of coherent detection.

### ***7.2.2 Coherent Optical Transceiver – Concepts and Building Blocks***

After a start of coherent system implementations with 40 Gbit/s in 2008, single carrier 100 Gbit/s DP-QPSK coherent systems have been shipped since 2010 [29]. In 2010 various modulation format options had been proposed for 100 Gbit/s applications [30], however, in the following years the optical transport market has rapidly accepted DP-QPSK with coherent reception due to its superior performance: Until today DP-QPSK had been massively deployed, it has reached a market share of more than 80%, and this is still growing.

The major driver of the 100G coherent transceiver commercialization was the OIF, which had initiated the “100G Ultra Long Haul DWDM Framework Document” [8] and component related documents [31, 32], with the intention of pushing interoperability and cost reduction by various implementation agreements in which the main building blocks of optical transceivers are described.

After 40 Gbit/s, 100 Gbit/s has been the 2nd bit rate hierarchy where client GE bit rates of 100GE [33] met optical transport client bit rates. The first commercially available 100 Gbit/s DP-QPSK transceiver operates at  $\sim 112$  Gbit/s transmission line rate or gross rate and  $\sim 28$  Gbd symbol rate or baud rate. Line rate and symbol rate are related via the modulation efficiency of 4 bits/symbol for DP-QPSK. The exact line rate is defined by the OTU4 line rate = 111.809973 Gbit/s given in G.709 [34], and the maximum net rate is defined by the 100GE rate [35]: 103.125 Gbit/s. The difference to the OTU4 line rate includes protocol overhead (OH) and 7% forward error correction (FEC) OH. If transceivers work on the OTU4 line rate, there is no

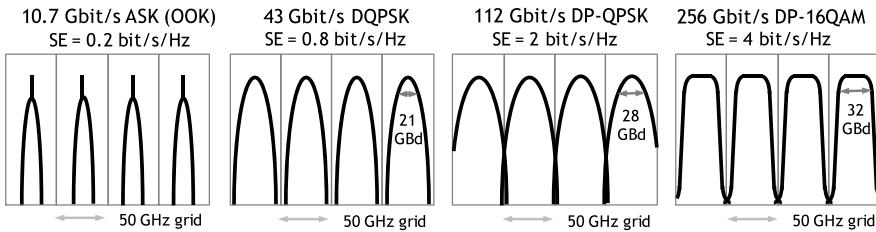


**Fig. 7.3** Channel allocation of bit rate hierarchies, showing *line rates* per carrier and modulation formats: four channels at 10.7 Gbit/s, 43 Gbit/s, 112 Gbit/s and 256 Gbit/s

capacity available for further bits potentially required for training sequences, for more details see Sect. 7.5.2, and the coherent receiver has to operate with blind adaptation. Transceivers from different suppliers operating on the OTU4 line rate are potentially interoperable if they include the same FEC encoding.

The 3rd hierarchy where GE rates meet transport bit rates will be 400 Gbit/s. It is targeted for 2018 and will support future 400GE rates [35] with a true net rate of 412.5 Gbit/s. 400 Gbit/s transceivers based on dual-carrier frequency division multiplexing (FDM) and DP-16QAM modulation format (8 bits/symbol) have been developed and entered the optical transport market in 2014 already. 16QAM modulation plus the higher line rate causes a degradation of about 10 dB in OSNR compared to 100 Gbit/s transceivers. In order to mitigate this penalty more powerful FEC has been developed (i.e. SD-FEC) leading to the 3rd FEC generation [36] (Sect. 7.4.2). The consequence of 400 Gbit/s transmission was the need for higher FEC overhead of  $\sim 25\%$  resulting in higher transmission line rates of 512 Gbit/s ( $2 \times 256$  Gbit/s FDM sub-carriers). The latter are based on 32 GBd symbol rate and can cope with bit error ratios (BER) before SD-FEC of 0.04.

The diagram most to the right in Fig. 7.3 shows the spectral characteristics of 400 Gbit/s transmitters based upon two FDM sub-carriers. For comparison purposes Fig. 7.3 also illustrates the spectral characteristics of commercially available 10 Gbit/s, 40 Gbit/s and 100 Gbit/s transceivers, from left to right, all on the 50 GHz channel grid. Figure 7.3 includes the respective spectral efficiencies, the line rates, the modulation formats, the symbol rates (GBd) in case of HOM formats (at 40 Gbit/s we exemplarily selected DQPSK), and the respective spectral efficiencies. The spectral efficiency is generally related to the information bit rate or net rate and the channel spacing (W). Spectral shaping or spectral pre-emphasis (cf. Section 7.5.1) has been applied for the 256 Gbit/s/32 GBd signals while the other signals in Fig. 7.3 are not spectrally pre-shaped.

Current 400 Gbit/s and next generations of optical coherent transceivers are based on the indispensable concepts of: HOM formats, polarization division multiplexing, FEC, digital-analogue and analogue-digital conversion, and DSP.

Polarization division multiplexing means transmission of data in both optical polarizations, thus PDM or dual polarization operation doubles the modulation efficiency and the spectral efficiency of any HOM format. DP operation of HOM became a common method together with coherent technology as fast and reliable



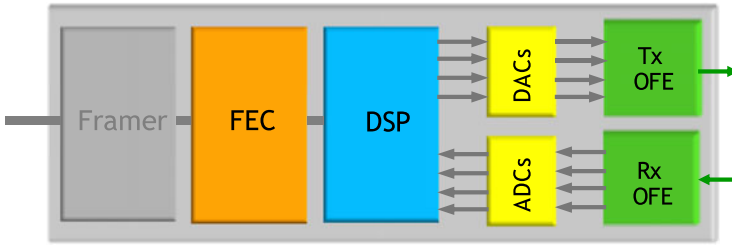


Fig. 7.4 Block diagram of a coherent transceiver

polarization demultiplexing became feasible by coherent detection and the following DSP.

A single carrier or FDM based optical transceiver with coherent detection as shown in Fig. 7.4 comprises four electronics and two optical building blocks: (1) the data framer as interface to client data structures, (2) FEC for data encoding and decoding, (3) the large DSP block including the HOM format generation and various algorithmic processing steps, (4) four DACs and four ADC data converters which support modulation and reception of the four tributaries:  $I_x$ ,  $I_y$ ,  $Q_x$  and  $Q_y$ , (5) the transmitter optical frontend (Tx-OFE) including linear amplification and modulation of light of a C-band tunable laser, and finally (6) the optical receiver frontend (Rx-OFE) consisting of a local oscillator (C-band tunable) and a coherent optical frontend.

A *Client data framer* realizes the mapping (multiplexing/demultiplexing) of variable length, higher-layer client signals (today mostly IP) over a circuit switched transport network like OTN [34]. Client interface considerations are beyond the scope of this chapter and will not be discussed further.

*Forward Error Correction (FEC)*: Transmitted data are encoded on an FEC encoder and the received and processed data are verified and corrected in an FEC decoder. FEC became inevitable in coherent transceivers as (a) error free transmission with BERs below  $10^{-15}$  cannot be achieved with coherent receivers and (b) high coding gain is required with high pre-FEC BERs above  $10^{-2}$  ensuring post-FEC BERs  $<10^{-15}$ . Due to the need and inclusion of SD-FEC, the FEC requires a significant part of the transceiver complexity and power consumption. More details about SD-FEC are reported in Sect. 7.4.

*Digital Signal Processing (DSP)*: DSP together with data converters are the key enablers of coherent technology. DSP comprises the implementation of all necessary algorithmic processing steps to recover single carrier related transmission impairments of a single fiber. However, space division multiplexing and transmission over multi-core fibers requiring massive  $M \times M$  MIMO algorithm implementations [18], related to  $M$  spatial coupled fiber modes and  $M$  polarization modes, will not be treated further in this chapter (but it is covered in detail in Chap. 1). Transmission over a single fiber on a single carrier with two polarizations reduces the MIMO space to a  $2 \times 2$  MIMO as applied at the polarization demultiplexing algorithm.

At the transmitter side the algorithms include encoding of bits onto HOM formats, spectral equalization and pre-emphasis which has become an important con-

cept for optimization of spectral efficiency. More details are given in Sects. 7.5.1 and 7.5.2. At the receiver side the most important algorithms required are: chromatic dispersion compensation, timing recovery, polarization demultiplexing, channel equalization, frequency and phase estimation adapted to HOM formats. Chromatic dispersion compensation requires high complexity at the receiver DSP due to the very high amount of dispersion of typically 35,000 ps/nm to be compensated. More details about the transceiver DSP are given in Sect. 7.5.

*High Speed Data Converters:* DACs and ADCs have enabled digital modulation and digital detection and have become inevitable interfaces to the optical frontends (OFE) of coherent transceivers. Due to the very high bit rates and the required complexity of DACs and ADCs, the digital revolution arrived in fiber optics several years later than in other technologies. More details on architectures and technologies of data converters are given in Sects. 7.6 and 7.7.3.

*Optical Frontends (OFE)* including the data modulator and polarization diversity receiver will be described in Sect. 7.7.

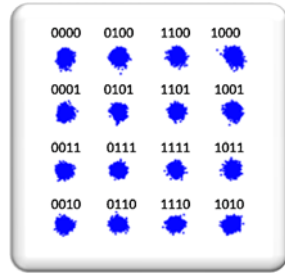
### 7.3 Higher-Order Modulation Formats

In electrical communication technologies very high constellation sizes up to 4096 ( $m = 12$ ) became standard applications but in optical communication the bit rates are significantly higher and the noise at the receiver is significantly lower and thus feasible constellation sizes for optical communication products are significantly smaller. However, a constellation size as high as 2048QAM including transmission over 150 km of fiber has already been demonstrated in fiber optics research [7]. The main challenges of applying high constellation sizes are laser phase noise and OSNR constraints, thus smaller constellations potentially up to 64QAM might be implementable in real systems in the near future and potentially up to 256QAM might be expected in about five to ten years. In this chapter we include constellation sizes up to 1024QAM for the comparison of HOM formats.

The main objective of HOM formats is to raise the spectral efficiency by increasing the bit rate together with keeping or reducing the modulation symbol rate and its signal spectral width. HOM formats are defined by their number of encoded bits on transmitted symbols. While in the standard NRZ modulation format 1 bit is encoded per symbol and the symbol rate corresponds to the bit rate, with HOM formats more bits are encoded per symbol so that the symbol rate and thus the spectral width of the modulated signal becomes significantly smaller than the bit rate.

Figure 7.5 shows exemplarily a 16QAM ( $M = 16$  symbols) constellation diagram of one polarization measured with a dual carrier DP-16QAM 512 Gbit/s transceiver. With 16QAM constellations 4 bits are encoded per symbol, as depicted in Fig. 7.5 with Gray mapped bits. Gray mapping [37] is a commonly applied mapping scheme that minimizes the number of bit errors between neighboring symbols as only 1 bit out of 4 is changed.

**Fig. 7.5** Measured 16QAM constellation diagram with Gray mapped bits



### 7.3.1 Quadrature Amplitude Modulation

The most commonly applied HOM formats are MQAM (multiple-quadrature-amplitude-modulation) formats, where  $M$  symbols have specific amplitude and phase states or in-phase ( $I$ ) and quadrature ( $Q$ ) components in the electric field as defined by their complex constellation diagram. The  $I$  and  $Q$  states have  $90^\circ$  phase difference and are modulated independently onto the same carrier.

According to information theory [38] the mapping of  $m$  bits onto the  $M$  symbols of HOM formats is referred to as coded modulation. The number  $M$  is the total number of symbols and determines the constellation size of an MQAM format. The number  $m$  of bits carried by each symbol is determined by:

$$m = R_C \times \log_2(M) \text{ [bits/symbol]} \tag{7.1}$$

$R_C$  represents the encoding rate or code rate which satisfies  $0 < R_C \leq 1$ . The channel encoder is adding a redundancy or a code OH to a stream of bits like forward error correction OH. The code overhead, usually given in percentage, is defined as:

$$\text{OH} = (1 - R_C)/R_C \tag{7.2}$$

In the absence of coding (code rate  $R_C = 1$ ) the total number of  $M$  different symbols is determined by:

$$M = 2^m \text{ [symbols]} \tag{7.3}$$

Each symbol is transmitted in a time slot  $T_S = 1/R_S$ , and the symbol rate  $R_S$  is related to the bit rate  $B$  following Hartley’s law [39]:

$$R_S = B/m \text{ [GBd]} \tag{7.4}$$

In (7.4)  $m$  represents a nominal spectral efficiency and determines the maximum number of bits per symbol,  $m$  is also denoted as modulation efficiency which is determined by the ratio of the bit rate  $B$  and the symbol rate  $R_S$ . We denote a modulation format as HOM format if more than only 1 bit is encoded per symbol, e.g. QPSK or “4QAM” encodes 2 bits/symbol.

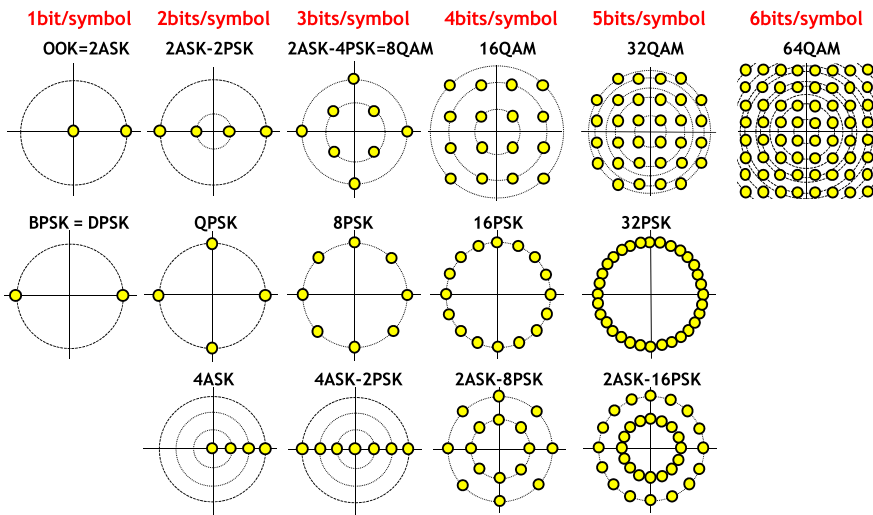


Fig. 7.6 Examples of constellation diagrams, the columns indicate respective numbers of bits/symbol

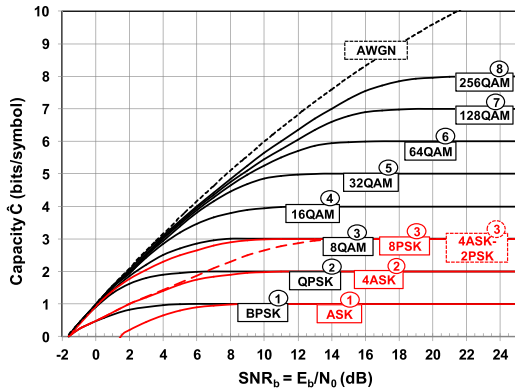
### 7.3.1.1 Constellation Diagrams

Figure 7.6 illustrates examples of QAM constellation diagrams including pure ASK (OOK) options (OOK and 4ASK) and various pure PSK formats, ASK-PSK combinations and MQAM options up to 64QAM. The columns indicate the modulation efficiencies by the number of  $m$  bits encoded per symbol. While a few examples of constellations consider only the real part or in-phase of the electric field, most constellations use the real and imaginary part, or in-phase ( $I$ ) and quadrature ( $Q$ ) of the electric field.

The first row of Fig. 7.6 starts with only one amplitude value modulated: this is standard NRZ-OOK or binary ASK or 2ASK encoding 1 bit/symbol ( $m = 1$ ). By adding a second amplitude and a second phase shifted by  $180^\circ$  we obtain 2ASK-2PSK which encodes 2 bits/symbol: as 00, 01, 10, 11. In the following constellation 2ASK-4PSK, corresponding to the conventional 8QAM format, 3 bits/symbol are encoded. The next constellations are square-16QAM, 32QAM and square-64QAM which were introduced in 1962 [40] and which encode 4, 5 and 6 bits/symbol, respectively.

The constellations of the second row of Fig. 7.6 show purely phase modulated signals. They all have one constant amplitude ring. Only the first two are of practical interest: BPSK (DPSK) and (D)QPSK which encode 1 and 2 bits/symbol, respectively. The following constellations from 8PSK to 32PSK are included here for illustration purposes only. The Euclidian distance or minimum distance between the symbols is a measure for the robustness of the constellations to noise, thus from left to right, especially visible for the constellations in row two, sensitivity to noise in-

**Fig. 7.7** Capacity in bits/symbol versus  $SNR_b$  for AWGN channels (Shannon limit) and for various modulation formats, numbers indicate maximum modulation efficiencies (bits/symbol). (Dashed red curve corresponds to 4ASK-2PSK)



creases significantly, so that BPSK has the highest robustness and 32PSK the lowest robustness to noise.

The constellation examples of the third row have up to four amplitudes and up to eight phase values. By 4ASK or Quaternary-ASK or 4PAM, 2 bits are encoded per symbol. All constellations of row three have significantly lower Euclidian distances than the constellations of the first row for corresponding modulation efficiencies.

### 7.3.1.2 Shannon Capacity Limit

HOM formats, that have widely been used in wireless and wireline and optical communication systems are square-MQAM formats, where the symbols are arranged in a square, leading to optimized Euclidean distances between the symbols which determine sensitivity performance or robustness versus noise.

According to Shannon [38] increasing the spectral efficiency by using higher constellation sizes of any HOM format comes at the price of higher signal to noise ratio (SNR) requirements. The Shannon-Hartley theorem describes that the ultimate capacity (limit)  $\hat{C}$  versus  $SNR_S$  (SNR per symbol) is given by a complex additive white Gaussian noise (AWGN) channel in the simple form of (7.5): For the same  $SNR_S$ , the capacity of any HOM format cannot be higher than the capacity of the AWGN channel.

$$\hat{C} = \log_2(1 + SNR_S) \text{ [bits/symbol]} \tag{7.5}$$

The Shannon capacity  $\hat{C}$  expresses error free transmission for the case of ideal channel coding and appears in the dimension of bits/symbol, as modulation efficiency. Figure 7.7 illustrates the Shannon capacity for the AWGN channel (limit) and includes the maximum achievable capacity (upper bound) of most HOM formats from Fig. 7.6, but including up to 256QAM formats versus  $SNR_b$  (per bit) according to [41, 42]. The difference between  $SNR_S$  and  $SNR_b$  is obtained by a comparison of (7.6) and (7.7), below.

Error free transmission is achieved in all cases if the  $SNR_b$  exceeds  $-1.59$  dB. As shown in Fig. 7.7, for sufficiently high  $SNR_b$  all formats saturate at their theoretical

maximum spectral efficiency, e.g. 4 bit/s/Hz for 16QAM, and at their theoretical maximum modulation efficiency of  $\log_2(M)$  bits per symbol. Comparison of formats with the same maximum capacity reveals that the formats modulating in one dimension only (4ASK) reach their maximum capacity at higher  $\text{SNR}_b$  than formats with modulation in both dimensions (QPSK). A comparison of 8QAM with 8PSK (red line) shows that 8QAM achieves higher capacity at lower  $\text{SNR}_b$ , in agreement with the observation of higher Euclidian distances of the constellation points of 8QAM compared to 8PSK.

It is interesting to note the following observation in Fig. 7.7: A specific target capacity, e.g. 5 bit/symbol, can be achieved with 32QAM at a high  $\text{SNR}_b > 12$  dB. Alternatively, one might use constellations larger than 32QAM and encode them with the appropriate code rate or redundancy to achieve a lower SNR requirement ( $\sim 9$  dB) for the same capacity. This is in contrast to the BER performance without coding, described in the following section where larger constellations sizes always require higher SNR than smaller constellations.

By including the nonlinear properties of the transmission fiber the theoretical maximum capacity of a fiber channel modulated with an HOM format is reduced as analyzed in [43]. These capacities have been denoted as the lower bound capacities.

### 7.3.1.3 BER Performance

According to communication theory [42] error probabilities can be calculated in terms of signal to noise ratio (SNR), which may be the SNR per bit ( $\text{SNR}_b$ ) or per symbol ( $\text{SNR}_S$ ), represented by (7.6) and (7.7):

$$\text{SNR}_S = E_S/N_0 \quad (7.6)$$

$$\text{SNR}_b = E_b/N_0 \quad (7.7)$$

with

$$E_b = E_S/m \quad (7.8)$$

$E_S$  and  $E_b$  are the energies per symbol and per information bit, respectively, and  $N_0$  is the corresponding noise power.

Figure 7.8 represents the theoretical electrical sensitivity performance of dedicated HOM formats in terms of their symbol error probability (SER) versus  $\text{SNR}_S$ , left diagram, and bit error probability or bit error ratio (BER) versus  $\text{SNR}_b$ , right diagram. Note, that the BER curves shown in Fig. 7.8 hold for the absence of coding ( $R_C = 1$ ).

BER versus  $\text{SNR}_b$  represents the more realistic case compared to SER versus  $\text{SNR}_S$ , as  $\text{SNR}_b$  takes into account how many bits are comprised and transported by a given symbol. For MQAM constellations and BER values smaller than 0.08 a good approximation for BER versus  $\text{SNR}_b$  can be found in [42] and is given by (7.9)

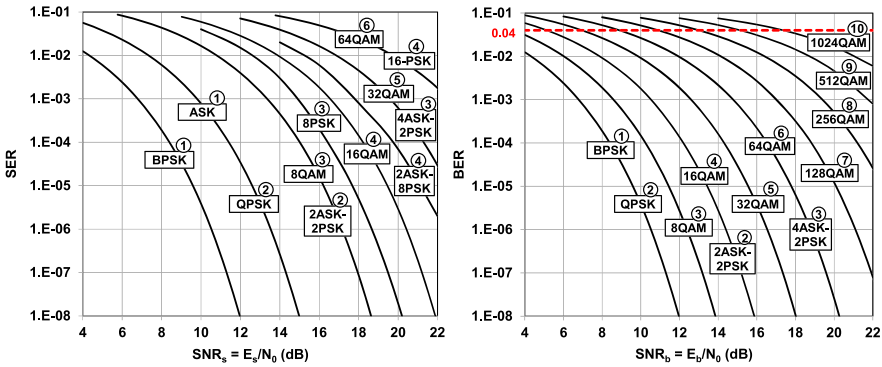


**Fig. 7.8** SER vs. SNR per symbol (*left*) and BER vs. SNR per bit (*right*) of various constellation diagrams, including the number  $m$  of modulation efficiency

$$BER = \frac{\sqrt{M} - 1}{\sqrt{M} \log_2(M)} \operatorname{erfc} \left( \sqrt{\left( \frac{3 \log_2(M)}{2(M-1)} \right) SNR_b} \right) \quad (7.9)$$

At first we compare the various HOM formats of Fig. 7.6 with respect to their symbol Euclidian distances in Fig. 7.8, left diagram, and focus on formats with equal modulation efficiency:

- (1) BPSK significantly outperforms ASK by about 3 dB lower  $SNR_b$ ,
- (2) QPSK outperforms 2ASK-2PSK,
- (3) 8QAM outperforms 8PSK and more significantly 4ASK-2PSK, as 8QAM has higher Euclidian distances between symbols, and
- (4) square-16QAM outperforms 2ASK-8PSK (star 16QAM).
- (5) A comparison of 64QAM with 16PSK, which perform both with similar Euclidian distances and SER versus  $SNR_s$ , demonstrates that 64QAM has a significant advantage as it encodes 2 bits/symbol more than 16PSK.

If we look into the diagram of BER versus  $SNR_b$  (right diagram of in Fig. 7.8) and take into account the number of bits ( $m$ ) each symbol is carrying, we can conclude that for the same  $SNR_b$  value square-MQAM formats perform with twofold higher modulation efficiencies compared to formats transporting symbols in a single state only: QPSK (2) versus BPSK (1); 16QAM (4) versus 2ASK-2PSK (2), and 64QAM (6) versus 4ASK/2PSK (3).

The main outcome of Fig. 7.8 is that the highest modulation efficiencies together with the best  $SNR_b$  performance are obtained with quasi square-MQAM constellation diagrams which outperform star-QAM and alternative ASK-PSK formats. Thus, MQAM formats became standard HOM formats and have received highest interest for optical transmission systems.

In order to compare the system sensitivities of HOM formats, their respective  $SNR_b$  at one common pre-FEC BER (e.g. of 0.04) can be used, as shown by the dashed red line in Fig. 7.8, right side. The BER of 0.04 is considered as an imple-

**Table 7.1** Signal to noise ratio per bit ( $SNR_b$ ) and OSNR values at 128 Gbit/s line rate versus number of bits per symbol ( $m$ ) of MQAM formats, required for 0.04 pre-FEC BER,  $SNR_b$  values at theoretical limit of pre-FEC BER

$m$ (bits/symbol)		2	3	4	5	6	7	8	9	10	
$SNR_b = E_b/N_0$ (dB)	@ pre-FEC BER	limit	1.1	2.6	4.2	5.9	7.7	9.6	11.5	13.5	15.6
		0.04	1.8	3.4	5.2	7.0	8.9	10.9	13.0	15.2	17.4
OSNR (dB) @ 128 Gbit/s		0.04	8.9	10.5	12.3	14.1	16.0	18.0	20.1	22.3	24.5

mentable pre-FEC BER of HOM formats with 25% SD-FEC OH with margin with respect to a theoretical limit, as described in more detail in Sect. 7.4.2.

The use of pre-FEC thresholds in case of SD-FEC has been questioned in [44] and generalized mutual information (GMI) has been suggested as a better predictor. However, for an SD-FEC OH of 25% which we consider throughout this chapter, it was also shown in [44] that deviations of pre-FEC BERs required in order to obtain a specific post-FEC BER appear to be rather small and are within the errors of SNR data which are summarized in Table 7.1.

Table 7.1 summarizes the required uncoded  $SNR_b(E_b/N_0)$  values versus the number  $m$  of bits/symbol of QPSK and square-MQAM formats related to a pre-FEC BER of 0.04 and at the theoretical limit of pre-FEC BER related to SD-FEC with 25% OH. Note, that the corresponding coded  $SNR_b$  values with 25% of OH would be 0.96 dB smaller. The estimated accuracy of the SNR values given in Table 7.1 is  $\pm 0.1$  dB up to  $m = 6$  (64QAM) and  $\pm 0.2$  dB for  $m$  between 6 and 10 (1024QAM).

The lower  $SNR_b$  values for the theoretical limits of per-FEC BER are apparently more optimistic compared to the higher  $SNR_b$  values at a constant pre-FEC BER of 0.04. For further comparison of HOM formats in this chapter we will consider only the  $SNR_b$  values at constant pre-FEC BER of 0.04. The differences or penalty steps of formats between QPSK ( $m = 2$ ) and 1024QAM ( $m = 10$ ) are about 2 dB, more precisely between 1.6 dB and 2.2 dB.

In optical communication, the optical signal to noise ratio (OSNR) is the parameter corresponding to the electrical parameter  $SNR_b$  [43] given by (7.10). The OSNR data are in reference to the gross bit rate or the line rate  $B_L$  including the coding with 25% of OH and the considered  $SNR_b$  values are, according to Table 7.1, the uncoded values at a BER of 0.04.

$$OSNR = B_L / (2 \times B_{ref}) \times SNR_b \quad (7.10)$$

$B_{ref}$  is the reference bandwidth, usually expressed as a 12.5 GHz (0.1 nm) bandwidth. The relation (7.10) is valid for single polarization as well as for dual polarization operation. For HOM formats with constant line rates, e.g. with constant FEC-OH, the OSNR penalties are identical to the  $SNR_b$  penalties and increase between the HOM formats roughly also in steps of 2 dB.



Table 7.1 includes the corresponding OSNR required for 128 Gbit/s line rate. The 8.9 dB of OSNR at 128 Gbit/s DP-QPSK will serve as OSNR reference throughout this chapter. The penalty of 15.6 dB between QPSK ( $m = 2$ ) and 1024QAM ( $m = 10$ ) is the price for the five-fold higher modulation efficiency.

### 7.3.1.4 Dual-Polarization MQAM



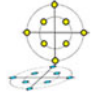
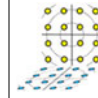
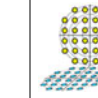
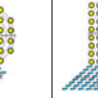
Polarization division multiplexing means transmitting data in two orthogonal optical polarizations ( $x$  and  $y$ ) which doubles the modulation efficiency and the spectral efficiency of any HOM format. PDM or dual polarization operation of HOM formats in combination with coherent technology has become a commonly applied method after coherent receivers have enabled fast and reliable digital polarization demultiplexing.

For the investigation of bit rates beyond 100 Gbit/s on a single carrier and multiple carriers as well we will focus in the following on standard HOM formats and will generally include PDM. Dual polarization operation simply multiplies the modulation efficiency according to  $m_{DP} = 2 \times m$ , and the granularity of  $m_{DP}$  for standard DP-MQAM formats appears in steps of 2 bits/symbol. Corresponding to this granularity, the theoretical OSNR penalty is usually considered to vary in steps of 2 dB. OSNR sensitivities determine the application area as 2 dB OSNR penalty results in 2 dB lower transmission distance. However, in practice the OSNR penalties are even higher than the theoretical OSNR predictions as HOM formats are usually associated with implementation penalties.

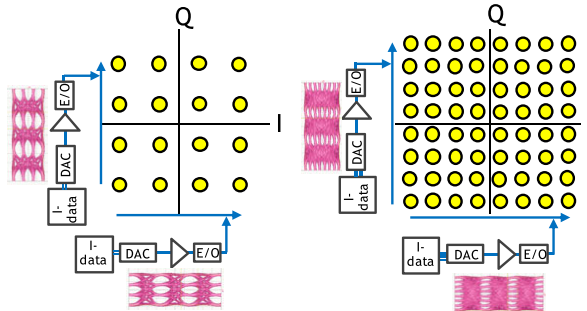
Table 7.2 illustrates the DP-BPSK and the DP-MQAM constellations up to DP-64QAM formats, including their modulation efficiencies  $m_{DP}$  expressed by the number of encoded bits per symbol. Table 7.2 includes the theoretical OSNR penalties of the DP-MQAM formats with BPSK and QPSK taken as a reference, for the case of SD-FEC with 25% OH and a pre-FEC BER of 0.04. The OSNR penalties versus HOM formats correspond to the  $SNR_b$  penalties according to (7.10) with the assumption of constant line-rate for all formats. The DP-MQAM formats illustrated in Table 7.2 are considered to be the most attractive ones for current and future generations of long haul and Metro transmission distances.

For transceivers operating with flexible adaption of the modulation format the 2 bits/symbol granularity of standard HOM formats is not always an optimum choice, and depending on the application finer granularities can be advantageous. Time domain hybrid modulation formats (TDHM) have been proposed [45–47] by generating so-called supersymbols with standard HOM format constellations alternating in the time domain. With this approach finer granularities can be obtained, e.g. 0.5 bits/symbol [48] and superior transmission performance has been demonstrated including filtering of Reconfigurable Optical Add Drop Multiplexers (ROADMs).

**Table 7.2** Dual-polarization BPSK and higher order modulation MQAM formats: DP-modulation efficiency  $m_{DP}$  (bits/symbol), constellations illustrated on both polarizations, OSNR penalties referenced versus DP-QPSK

	HOM format					
	DP-BPSK	DP-QPSK	DP-8QAM	DP-16QAM	DP-32QAM	DP-64QAM
$m_{DP}$ (bits/symbol)	$2 \times 1$	$2 \times 2$	$2 \times 3$	$2 \times 4$	$2 \times 5$	$2 \times 6$
DP-constellation						
OSNR penalty (dB)	0	0	1.6	3.4	5.2	7.2

**Fig. 7.9** 16QAM generation with 4 level modulator driving signals (*left*) and 64QAM generation with 8 level modulator driving signals using a single IQ modulator



**7.3.1.5 Principle of DP-MQAM Modulation and Reception**

A 16QAM signal in optical transmission by modulating a single IQ modulator with a 4-level drive signal (4PAM signal) has been demonstrated in 2008 [49] and together with a 6-bit DAC in 2010 [50], and a 64QAM signal has been generated with an 8-level drive signal (8PAM signal) using a DAC with only 3 bit resolution [51].

The examples in Fig. 7.9 depict the principle of generating e.g. 16QAM or 64QAM constellations by a 2-bit DAC ( $2^2 = 4$  signal levels) or by a 3-bit DAC ( $2^3 = 8$  signal levels), respectively, with a single polarization IQ modulator as E/O converter. The levels or number of states of the electrical driving signals correspond to the number of projections of the symbols onto the in-phase and the quadrature axis. The I/O modulator acts as a PAM to QAM converter. Each symbol of the complex electrical output field of the transmitter is addressable, provided that the chain DAC-driver-modulator is highly linear.

With one IQ modulators per polarization, the  $I$  and  $Q$  components of both, the optical  $x$ - and  $y$ -polarization, can be generated at the transmitter output resulting in a quasi 4D modulation format by 4 different optical fields [52].

High speed DACs implemented in ASICs (see Sect. 7.7.3) of deployed optical transceivers have a limited resolution between 6 and 8 bits and support sampling rates between 32 and 64 GSamples/s, and very recently up to 92 GSamples/s. For

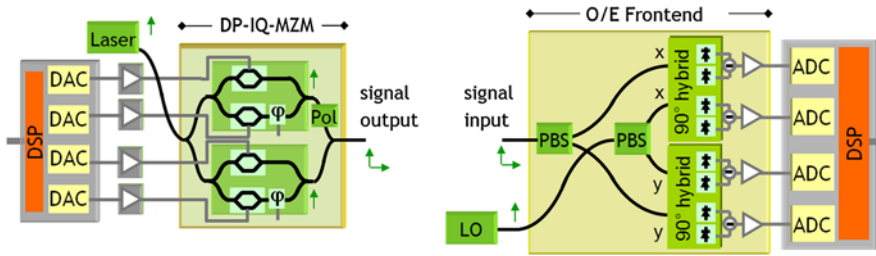


**Fig. 7.10** Transmitter and receiver setup with IQ modulator and receiver details (schematic),  $\varphi$ : 90° phase shifter; PBS: polarization beam splitter

measurement equipment DACs with 10 bit and more are available which support sampling rates up to a few GSamples/s. The effective number of bits (ENOB) is typically 1 to 3 bits lower than the theoretical resolution. In the case of SiGe based 6 bit DACs the ENOB is  $\sim 5$  bits and for CMOS based 8 bit DACs the ENOB is in the range of 4.5 to 6 bits. Table 7.3 compiles the analogue modulation levels of the DAC output and the minimum DAC resolution required to encode various standard HOM formats. The modulation efficiency  $m_{DP}$  (bits/symbol) includes polarization multiplexing or dual-polarization operation.

Figure 7.10 shows the schematics of a state-of-the-art DP-MQAM transmitter and a coherent receiver. The transmitter includes DSP, four DACs for four tributaries and a dual polarization I/O modulator on the basis of two nested Mach-Zehnder modulators (MZM) per polarization, described in more detail in Sect. 7.7.1. The transmitter includes a C-band tunable laser in an integrated tunable laser assembly (ITLA).

Four parallel linear amplifiers are required after the DAC to amplify their output of typically 1V differential to  $\sim 6V_{pp}$  ( $\sim 2V_{\pi}$ ) single ended as required at the modulator input.

An MZM has sinusoidal electrical field modulation characteristics and not linear as required for PAM to QAM conversion. Two alternative approaches are applied to compensate or counteract the shortcomings of the MZM characteristics: (a) pre-compensation of the multi-level driving signals with DACs and modulation with non-equidistant levels, (addressed in Sect. 7.5.1), or (b) modulation with lower amplitude of  $\sim V_{\pi}$  or even less, so that the MZM is operated in the quasi linear regime. This approach results in higher insertion loss as the lowest insertion loss under modulation is obtained only when the modulator is driven with the full  $2V_{\pi}$  modulation amplitude.

The receiver also shown in Fig. 7.10 includes an LO laser and the polarization diversity O/E frontend. Key elements of the latter are polarization beam splitters (PBS) and optical 90° hybrids which enable interference of the signal, in phase and quadrature components in  $x$ - and  $y$ -polarization, with the light of the LO laser, and four balanced photodiodes which convert the received signal spectrum to the electrical baseband, linear TIAs, (for more details see Sect. 7.7.2), and four ADCs for conversion of the four tributaries followed by the receiver DSP, to be discussed in more detail in Sect. 7.6.2.

### 7.3.2 Spectral Efficiency and Fiber Capacity

After 2009, with the availability of high resolution high speed DACs, significant progress in research has been made with the demonstration of HOM formats and constellation sizes of 16QAM and beyond targeting very high spectral efficiencies and very high capacities on a single fiber. By using DP-16QAM an SE of 6.4 bit/s/Hz and a very high fiber transmission capacity of 69.1 Tbit/s was demonstrated [16], and with DP-36QAM, a non “standard” HOM format which has a non integer modulation efficiency by encoding 10.34 bits/symbol, the SE was increased to 8 bit/s/Hz and the demonstrated fiber transmission capacity was 64 Tbit/s [53]. In both experiments the SE was supported by appropriate wavelength interleavers and a WDM crosstalk penalty was tolerated. Finally, the high capacities were achieved including L-band transmission.

With DP-64QAM [54, 55] the spectral efficiency has been further increased and including FDM 10 bit/s/Hz has been reported [56]. A transmission capacity of 45 Tbit/s using the C-band only has been achieved including spectral shaping to minimize the linear WDM crosstalk. By moving to DP-128QAM, a spectral efficiency of 11 bit/s/Hz has been demonstrated and an extremely high fiber transmission capacity of 101.7 Tbit/s including L-band transmission was reported. In all high capacity WDM transmission experiments mentioned above an HD (hard decision) -FEC with 7% OH has been included.

Even higher constellation sizes and spectral efficiencies have been achieved by DP-256QAM enabling a spectral efficiency of 11.8 bit/s/Hz [57], by DP-512QAM resulting in a spectral efficiency of 13.2 bit/s/Hz [58], by DP-1024QAM with 13.8 bit/s/Hz SE [6] and finally by DP-2048QAM with the record spectral efficiency in optical transmission of 15.3 bit/s/Hz [7] without use of SDM. The highest constellation sizes have been obtained using arbitrary waveform generators (AWG) including DACs with 10 bit theoretical resolution operated at 12 GSamples/s. These DACs support low symbol rates ( $\sim 6$  GBd) only and thus very narrow linewidth lasers are required as well. As these narrow linewidth lasers are available only for a limited number of wavelengths, no DWDM experiments and no new record capacities could be demonstrated so far based upon the highest constellation sizes. In the transmission experiments with particularly high constellation sizes the OSNR constraints were mitigated by Raman amplification. Table 7.4 summarizes selected high capacity experiments with modulation formats between DP-16QAM and DP-128QAM [59] and compiles the various parameters for comparison: the modulation efficiency  $m_{DP}$ , the spectral efficiency SE, the total fiber transmission capacity achieved, the line rate ( $B_L$ ), the applied number of sub-carriers for the case of FDM, the symbol rates ( $R_S$ ), the net rate ( $B_N$ ), the channel spacing ( $W$ ), the bandwidth efficiency  $\eta$  (described below by (7.13)) and the corresponding C- and L-band fiber bandwidths.

For the selected experiments in Table 7.4 the modulation efficiency and spectral efficiency, the bit rates and symbol rates, the number of sub-carriers and the C- and the L-band bandwidths vary significantly. Only the FEC OH remains constant and the bandwidth efficiency  $\eta$  remains comparable.

**Table 7.3** DAC output levels and minimum required DAC resolution versus HOM formats

	HOM format									
	DP-QPSK	DP-8QAM	DP-16QAM	DP-32QAM	DP-64QAM	DP-128QAM	DP-256QAM	DP-512QAM	DP-1024QAM	
$m_{DP}$ (bits/symbol)	4	6	8	10	12	14	16	18	20	
Analogue modulation levels	2	4	4	6	8	12	16	24	32	
Minimum resolution (bit)	1	2	2	2.6	3	3.6	4	4.6	5	

**Table 7.4** Overview of high capacity experiments with key performance parameters for comparison

Format	$m_{DP}$ (bits/symbol)	SE (bit/s/Hz)	Cap. (Tbit/s)	$B_N$ (Gbit/s)	$B_L$ (Gbit/s)	FEC OH (%)	no sub- carriers	$R_s$ (GBd)	Grid W (GHz)	$\eta$ (GBd/GHz)	C-band (THz)	L-band (THz)	Ref.
DP16QAM	8	6.4	69.1	160	171	7	1	21.66	25	0.87	4.3	6.7	[16]
DP-36QAM	10.34	8	64	100	107	7	1	10.7	12.5	0.86	4.0	4.2	[53]
DP-64QAM	12	10	45.2	500	538	7	8	5.6	50	0.90	4.5	0.0	[56]
DP-128QAM	14	11	101.7	275	294	7	4	5.25	25	0.84	4.8	4.6	[59]

In the following part of this section we will compare potential spectral efficiencies and total fiber capacities of HOM formats for an optical C-band fiber bandwidth of 4.4 THz and exclude L-band transmission. We will not discuss potential application areas and consider constellation sizes between DP-QPSK and DP-1024QAM, we will include throughout 25% OH for SD-FEC, to counteract OSNR constraints of HOM. Our transmission line rates are generally 28% higher than the net rates, e.g. 128 Gbit/s and 100 Gbit/s, respectively while the true net rates are always  $\sim 3\%$  above our depicted net rates, as we include GE rates of e.g. 103.125 Gbit/s. As we consider 25% of FEC OH, the SE will be correspondingly smaller than achievable with 7% OH only.

Symbol rates and bit rates of HOM formats are linked via Hartley's law (7.4) and using modulation efficiencies in dual polarization operation ( $m_{DP}$ ) symbol rates  $R_S$  as given by (7.4) are modified by:

$$R_S = B_L/m_{DP} \quad (7.11)$$

$B_L$  is the transmission line rate and the transported net rates  $B_N$  and the channel spacing ( $W$ ) determine the spectral efficiencies (SE) according to:

$$SE = W/B_N \quad (7.12)$$

In DWDM transmission the channel allocation scenarios are described by the bandwidth efficiency parameter  $\eta$  given by:

$$\eta = R_S/W \quad (7.13)$$

According to [60] DWDM channel allocation scenarios are distinguished and designated as:

- (1)  $\eta > 0.2$ : legacy WDM or coarse WDM
- (2)  $0.2 > \eta > 0.83$ : common DWDM
- (3)  $0.83 > \eta > 1.0$ : quasi Nyquist WDM
- (4)  $\eta = 1$ : Nyquist WDM
- (5)  $\eta > 1$ : super-Nyquist-WDM (faster than Nyquist)

For the fiber capacity discussion in this chapter we will focus on three different cases of DWDM bandwidth efficiency with the following terminology:

$$\eta \approx 0.64: \text{ "far Nyquist DWDM"} \quad (7.14)$$

$$\eta \approx 0.85: \text{ "near Nyquist DWDM"} \quad (7.15)$$

$$\eta = 1: \text{ "Nyquist DWDM"} \quad (7.16)$$

For example, "far Nyquist" DWDM (7.14) corresponds to a 50 GHz channel grid with a transmitted format of 32 GBd symbol rate, e.g. using 128 Gbit/s DP-QPSK, as also illustrated in Fig. 7.11, left side. The center and right side of Fig. 7.11 represent "near Nyquist" DWDM (7.15) cases with 32 GBd symbol rate on a 37.5 GHz grid

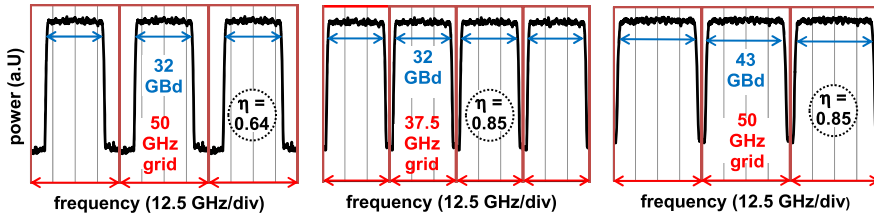


**Fig. 7.11** Illustration of “far-Nyquist DWDM” (left) and “near Nyquist DWDM” (center and right) with 32 GBd and 43 GBd of symbol rates

and with 43 GBd on a 50 GHz grid, respectively. 50 GHz is the standard ITU-T channel grid and 37.5 GHz an example of a flexible channel grid with a granularity of 12.5 GHz [61]. In all three examples of Fig. 7.11 the signals are spectrally pre-shaped and show no linear crosstalk, more details will be given in Sect. 7.5.1.1.

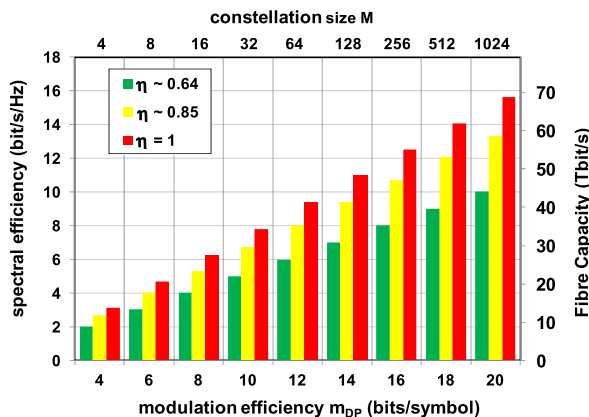
The gain of spectral efficiency and capacity by going from “far-” to “near Nyquist DWDM” and to “Nyquist DWDM” are 33% and 56%, respectively. Further capacity advantages potentially feasible with “faster than Nyquist” ( $\eta > 1$ ) approaches will not be considered here.

The bandwidth efficiency is a very sensitive measure for the routing capabilities of transmitted formats and determines the acceptable number of ROADMs included in a transmission link [48]. In case of  $\eta \approx 0.64$  many ROADMs ( $> 10$ ) can be passed, while for  $\eta \approx 0.85$ , only a few ( $< 4$ ) can be included.

Figure 7.12 illustrates the full range of spectral efficiencies and maximum single fiber transmission capacities in the optical C-band (4.4 THz) available with DP-MQAM formats, indicated versus constellation size  $M$  or modulation efficiency  $m_{DP}$ . The SE and capacity data are bit rate independent and can be considered for single carrier solutions as well as for FDM or superchannel solutions [60].

At far Nyquist DWDM ( $\eta \sim 0.64$ ) the SE (capacity) increases with the constellation size from 2 bit/s/Hz (8.8 Tbit/s) to 10 bit/s/Hz (44 Tbit/s) with DP-QPSK and DP-1024QAM, respectively. At Nyquist DWDM ( $\eta = 1$ ), the SE (capacity) in-

**Fig. 7.12** Spectral efficiency and C-band fiber capacity versus  $M$  or  $m_{DP}$  of DP-MQAM formats with bandwidth efficiencies of  $\eta \sim 0.64$  (green-),  $\eta \sim 0.85$  (yellow-) and  $\eta = 1$  (red bars)



creases from 3.1 bit/s/Hz (13.8 Tbit/s) to 15.6 bit/s/Hz (69 Tbit/s), and at the intermediate case of near Nyquist DWDM ( $\eta \sim 0.85$ ), the SE (capacity) increases from 2.7 bit/s/Hz (11.7 Tbit/s) to 13.3 bit/s/Hz (59 Tbit/s).

Any future gain of spectral efficiency and fiber capacity which may be potentially realized in the future with “faster than Nyquist” will scale with the achieved bandwidth efficiency. If transmission within the L-band is also included, the total fiber transmission capacity of HOM formats can be further increased, as illustrated by three experimental demonstrations included in Table 7.4, with as much as about 150% capacity increase reported in [16].

### 7.3.3 High Bit Rate Transmission

According to Hartley’s law (7.4) implementation of HOM formats is a promising approach for achieving very high bit rates (line rates) provided sufficiently fast electronics are available. Table 7.5 is a compilation of research demonstrators from the last few years where symbol rates beyond 40 GBd have enabled to achieve the highest line rates realized on a single carrier so far. The examples include different formats and modulation efficiencies ( $m_{DP}$ ), different DAC approaches and technologies, different net rates and spectral efficiencies, different FEC OH and different experimentally achieved OSNR values for the given FEC thresholds.

Table 7.5 shows that significant progress in research has been achieved to obtain single carrier line rates of 400 Gbit/s [62] and beyond in order to approach the 1 Tbit/s net rate which has finally been achieved in 2015 with a line rate of 1.24 Tbit/s reported in [63]. However, this result may be questioned to be a true single carrier 1 Tbit/s demonstration as the Nyquist shaped 124 GBd signal has been synthesized from four 32.5 GHz spectral sub-bands (spectral slices) merged into a 125 GHz frequency slot.

The two research demonstrators in Table 7.5 using a “DAC resolution” of 2 bits were applying a passive combination of binary data to obtain a 4PAM signal for the 16QAM generation [64, 65]. The demonstrator in Table 7.5 with a 3-bit DAC applies an InP based power-DAC [66]. The demonstrators in Table 7.5 close to products including high resolution DACs with more than 6 bits theoretical resolution are: 552 Gbit/s transmission [67] with 46-GBd DP-64QAM using 65-GSample/s DACs with 8 bit theoretical resolution in CMOS technology, 864 Gbit/s transmission [68] with 72-GBd DP-64QAM with a SiGe DACs, and finally the 1240 Gbit/s demonstrator with 124 GBd DP-32QAM using also the 65-GSamples/s DACs with 8 bit theoretical resolution in CMOS technology, but required in total 16 DACs while a true single carrier and single sub-band transceivers would include only 4 DACs for the 4 tributaries.

Single-carrier 1 Tbit/s solutions combine high constellation sizes [73] together with ultimate symbol rates [74], while few carriers 1 Tbit/s solutions [69–74] are based upon the superchannel concept [60] targeting the use of two, three or four FDM sub-carriers, that the requests on constellation size or symbol rate become



less demanding. The first commercially available 100 Gbit/s transceiver introduced in 2009 uses a two sub-carrier FDM solution based on the first 40 Gbit/s coherent receiver technology using the DP-QPSK modulation format. Current 400 Gbit/s transceivers introduced in 2014 also use two sub-carrier FDM but with DP-16QAM modulation format providing a 2-fold higher spectral efficiency than DP-QPSK which raises the SE from 2 bit/s/Hz to 4 bit/s/Hz.

The superchannel or FDM concept cannot provide higher spectral efficiencies than single carrier solutions and therefore superchannels are considered as an intermediate stage only. The final target is a single carrier transceiver which will be more cost-effective and will have less components and lower power consumption. The higher symbol rates of single carrier implementations match better with the granularity and the spectral properties of optical routing components. While the first single carrier 100G transceiver was available only one year after the two sub-carrier FDM product, the product maturity of a single carrier 400G transceiver e.g. based on DP-16QAM with 64 GBd symbol rate will require a longer development time. The development of a single carrier 1 Tbit/s transceiver is significantly more demanding, as the symbol rate or the modulation efficiency has to be 2.5 times higher than for a 400G single carrier solution.

In the following part of this section we will investigate potential future 400 Gbit/s single carrier product implementations, address the particular challenge of 1 Tbit/s single carrier options, and compare the performance of 400 Gbit/s solutions with dual and single carrier(s) in detail, and finally depict realistic scenarios for 1 Tbit/s few carrier product options.

### 7.3.3.1 400G and 1T Single Carrier Options

Table 7.6 illustrates the symbol rate correlation and OSNR penalties of MQAM HOM formats for 400 Gbit/s net rate, based upon 512 Gbit/s line rate with 25% SD-FEC OH. Symbol rates supported by corresponding transceivers are mainly limited by the data converters (DACs and ADCs) and to a lower extent by the O/E converters as modulators and receivers have already been demonstrated to operate at symbol rates higher than 64 GBd [71]. The MQAM constellation sizes shown range from QPSK (4 bits/symbol) up to the 1024QAM (20 bits/symbol), and dual-polarization operation is generally included.

As already indicated in Table 7.1 for  $SNR_b$ , the OSNR penalty for 512 Gbit/s or any other constant bit rate exhibits a difference of about 2 dB between adjacent standard MQAM formats. The colors at the symbol rates in Table 7.6 indicate the probability of the data converter availability within the next 5 to 10 years (red: unlikely, orange: likely; green: currently available). Symbol rates up to 32 GBd are supported by current DAC and ADC technologies implemented in commercial 100 Gbit/s and 400 Gbit/s transceivers. DAC technologies available in 2015 [75] support symbol rates of at least 43 GBd, but symbol rates above 70 GBd appear to be very challenging for data converters with more than 6 bits of theoretical resolution. Apparently, the current main development targets of the data converter industry are to reduce

**Table 7.5** Examples of high line rate transmission experiments with symbol rates >40 GBd

Line rate (Gbit/s)	Format	Symbol rate (GBd)	DAC res. (bits)	$m_{DP}$ (bits/symbol)	Net-rate (Gbit/s)	SE (bit/s/Hz)	FEC OH (%)	FEC thresh. (BER)	OSNR exp. (dB)	WDM chs (no.)	Reach (km)	Ref.
428	DP-QPSK	107	-	4	400	2.9	7	0.0038	19.2	8	5600	[62]
516	DP-64QAM	43	3	12	400	8	20	0.02	27.5	20	600	[66]
552	DP-64QAM	46	8	12	334	6.7	58	0.09	21.5	153	2000	[67]
640	DP-16QAM	80	2	8	520	5.2	23	0.03	22.3	10	3200	[64]
856	DP-16QAM	107	2	8	713	5.9	20	0.019	26	5	200	[65]
864	DP-64QAM	72	6	8	640	6.4	35	0.04	27.5	1	400	[68]
1240	DP-32QAM	124	8	10	1000	8	24	0.042	31.5	1	660	[63]

**Table 7.6** Combinations of HOM formats and symbol rates enabling 512 Gbit/s line rate on a single carrier; colors at symbol rates indicate (expected) data converter availability: red: unlikely within next 5–10 years, orange: likely; green: available. OSNR penalties given with 128 Gbit/s DP-QPSK as reference

	HOM format									
	512 Gbit/s – 1 carrier									
$m_{DP}$ (bits/symbol)	DP-QPSK	DP-8QAM	DP-16QAM	DP-32QAM	DP-64QAM	DP-128QAM	DP-256QAM	DP-512QAM	DP-1024QAM	
4	6	8	10	12	14	16	18	20		
Symbol rate (GBd)	128	85	64	51	43	37	32	28	26	
OSNR penalty (dB) <sup>a</sup>	6.0	7.6	9.4	11.2	13.1	15.1	17.2	19.4	21.6	
	Longhaul									Metro
										Data center
										???

<sup>a</sup> 128 Gbit/s DP-QPSK

power consumption of DACs and ADCs while to increase their sampling speed has lower priority.

On the other hand, in research significantly higher symbol rates such as 80 to 107 GBd [74] have already been reported from experiments in which a passive combination of binary data have enabled to obtain 100 GBd four level signals. For commercial products high resolution DACs become mandatory in order to optimize the spectral efficiency by pulse shaping which requests additional 2 to 3 bits of DAC resolution (for details see Sect. 7.5.1).

As an example, we will compare two DP-MQAM format options which both enable 400 Gbit/s on a single carrier. According to Table 7.6 these are 64 GBd symbol rate with 16QAM or 32 GBd symbol rate with 256QAM, and they differ by a factor of two in modulation efficiency and capacity: DP-16QAM with 8 bits/symbol and DP-256QAM with 16 bits/symbol. The second option has about 8 dB higher OSNR requirement and in addition a 3 dB lower robustness to SPM [12] due to half the symbol rate compared to the first option. The price for the 2-fold higher capacity is about 11 dB penalty in transmission performance or more than 90% of transmission reach reduction. Therefore the second option might be attractive for shorter reach and future data center communication while the first option is an attractive 400G single carrier transceiver solution for longer reach applications. Finally we will shortly look on the very challenging 1 Tbit/s options on a single carrier, as depicted in Table 7.7. The realization of 1 Tbit/s on a single carrier and with a single sub-band might be feasible only with the three HOM options highlighted in orange, however, by what time or whether at all will primarily depend on the future progress of data converters. Moreover, as these options have significant OSNR penalty, they are expected to be suitable for short reach applications only.

### 7.3.3.2 Transmission Reach of 400 Gbit/s Single Carrier and Dual Carrier FDM

In this section we will analyze the transmission reach performance of 400 Gbit/s single and dual carrier FDM options ( $2 \times 200$  Gbit/s) over dispersion uncompensated fiber. As in the previous section the line rate will be kept constant at 512 Gbit/s with 25% FEC OH, and the symbol rates will vary with the HOM formats. As a reference we will take again the performance of 2nd generation 100 Gbit/s transceivers with 128 Gbit/s line rate and 32 GBd DP-QPSK including 25% OH, related to a pre-FEC BER of 0.04.

We will limit the maximum constellation size to 256QAM and consider transmission over dispersion uncompensated fiber links where the statistics of HOM can be described by Gaussian noise (GN) [76]. We will also assume that differences in nonlinear impairments from constellation sizes can be neglected and that the transmission performance can be described by the GN [77] or the enhanced GN model [78].

Independent of the transmission format and optical fiber type, transmission distances achievable with EDFA repeaters over  $N$  spans of fiber are determined by

**Table 7.7** Combinations of HOM formats and symbol rates for 1280 Gbit/s line rate on a single carrier; colors at symbol rates indicate (expected) data converter availability: red: unlikely (during the next 5 to 10 years), orange: likely; OSNR penalties are given relative to those of 128 Gbit/s DP-QPSK

	HOM format 1280 Gbit/s – 1 carrier									
	DP-QPSK	DP-8QAM	DP-16QAM	DP-32QAM	DP-64QAM	DP-128QAM	DP-256QAM	DP-512QAM	DP-1024QAM	
$m_{DP}$ (bits/symbol)	4	6	8	10	12	14	16	18	20	
Symbol rate (GBd)	320	213	160	128	107	91	80	71	64	
OSNR penalty (dB) <sup>a</sup>	10.0	11.6	13.4	15.2	17.1	19.1	21.2	23.4	25.6	

<sup>a</sup> 128 Gbit/s DP-QPSK

amplified spontaneous emission (ASE) noise accumulation and the received OSNR. Measured with 0.1 nm resolution bandwidth, OSNR is for instance given by [79]:

$$OSNR (0.1 \text{ nm}) [\text{dB}] = P_F - \alpha_F - NF - 10 \log(N) + 58 \text{ dB} \quad (7.17)$$

Equation (7.17) assumes constant fiber launch power ( $P_F$ ) into each fiber span, constant fiber attenuation ( $\alpha_F$ ) of each span, and constant noise figure ( $NF$ ) of each repeater amplifier. In order to achieve a targeted BER (e.g. of 0.04) after transmission with a specific modulation format over a specific type of fiber, the achievable transmission distance  $D_N$  (7.18) or the number of spans  $N$  are determined only by the OSNR receiver sensitivity ( $OSNR_{RX}$ ) and the optimum fiber launch power ( $P_{opt}$ ) into each transmission fiber span  $N$ :

$$D_N [\text{dB}] = 10 \log(N) \propto P_{opt} - OSNR_{RX} \quad (7.18)$$

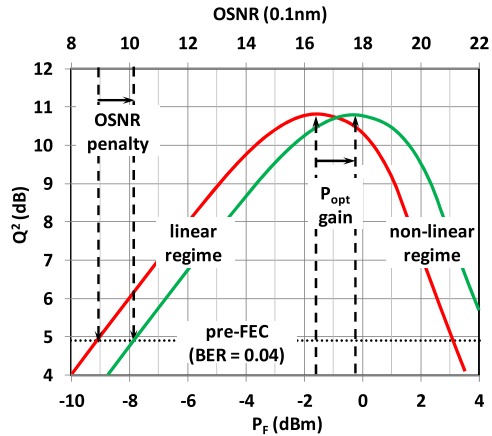
The required OSNR sensitivities (penalties) scale with the bit rates according to (7.10) and with the constellation size of HOM formats, as e.g. shown in Table 7.6 for 400 Gbit/s net rate. The optimum launch power for dispersion uncompensated transmission with HOM formats is dominated by intra-channel nonlinear effects [12]. These depend on the spectral shape and the spectral width of the transmitted symbol rate. In a simplified picture we assume that  $P_{opt}$  doubles (3 dB  $P_{opt}$  gain) if the symbol rate is doubled. According to (7.18) we simply can express the transmission reach penalty by the OSNR penalty and the  $P_{opt}$  penalty or gain. Inter-channel nonlinear effects at uncompensated transmission are not negligible but of minor importance and will not be considered in this chapter.

In Fig. 7.13 we illustrate the transmission performance over a few spans of dispersion uncompensated SMF fiber at two different bit rates (red and green curves) by their respective  $Q^2$  factor versus  $P_F$  and OSNR. The  $Q^2$  factors are calculated from the BERs according to [79] and the OSNR is related to  $P_F$  according to (7.17). In both cases we have significant  $Q^2$  factor margins above  $Q^2 \sim 4.9$  dB as BERs are lower than the targeted pre-FEC BER of 0.04. In the low  $P_F$  regime (below -4 dBm) both cases perform in the linear transmission regime where the  $Q^2$  factor increases linearly with  $P_F$ . The linear increase of the  $Q^2$  versus OSNR represents the back-to-back performance of the case with  $OSNR_{RX}$  obtained at  $Q^2 \sim 4.9$  dB ( $BER = 0.04$ ). In the high  $P_F$  regime (above +3 dBm) both cases perform in the non-linear transmission regime where the  $Q^2$  factor decreases with  $P_F$ . Optimum transmission performance is obtained in between where  $P_{opt}$  at highest  $Q^2$  factors (lowest BERs) are obtained, respectively. The two cases show different  $OSNR_{RX}$  and different  $P_{opt}$ , but their differences in terms of OSNR penalty and  $P_{opt}$  gain appear comparable. Thus both cases perform with comparable transmission reach.

In the following part of this section we will analyze 400 Gbit/s and 1 Tbit/s options of HOM formats with respect to their transmission reach penalty (reach reduction) versus our reference format 128 Gbit/s DP-QPSK.

A comparison of the single carrier performances at 200 Gbit/s (a) and 400 Gbit/s (b) at the same HOM format shows: (a) has 3 dB lower OSNR sensitivity compared to (b), while (b) supports 3 dB higher launch power compared to (a) due to the

**Fig. 7.13**  $Q^2$  factor versus fiber launch power ( $P_F$ ) for two different bit rates cases (red and green curves) with respective OSNR penalty and  $P_{opt}$  gain

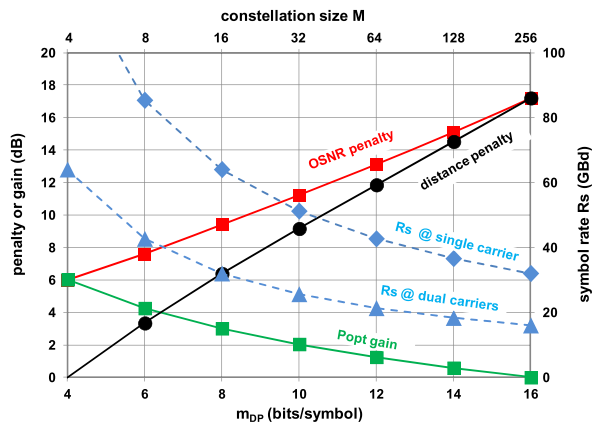


twofold higher symbol rate and spectral width as well. Thus both solutions have the same transmission reach, and the same reach is obtained also for  $2 \times 200$  Gbit/s as a dual carrier FDM option for 400 Gbit/s is compliant with  $2 \times 200$  Gbit/s DWDM channels.

The dual carrier FDM option has the same OSNR sensitivity and the same  $P_{opt}$  as the single carrier 400 Gbit/s option because the bit rate and the total power  $P_{opt}$  are identical. As a consequence distance penalties of HOM formats are independent of the transmission bit rate and independent of the number of FDM sub-carriers. In Fig. 7.14 we display OSNR penalty,  $P_{opt}$  gain and reach penalty of single and dual carrier 400 Gbit/s options together with their symbol rates as a function of the constellation size of the MQAM HOM format. 128 Gbit/s DP-QPSK with 32 GBd symbol rate is taken as the reference for the penalty values shown.

Compared to the previously introduced  $SNR_b$  and OSNR penalty versus constellation size which increases by steps of  $\sim 2$  dB between the standard MQAM formats ( $\Delta m_{DP} = 2$ ), the reach penalty increases more significantly between the

**Fig. 7.14** Reach penalty, OSNR penalty,  $P_{opt}$  gain and symbol rates per carrier versus constellation size for single and dual carrier 400 Gbit/s solutions, penalty and gain values given relative to those of 128 Gbit/s DP-QPSK (32 GBd)



standard MQAM formats by steps of  $\sim 3$  dB due to the optical gain ( $P_{opt}$ ) which varies by steps of  $\sim 1$  dB.

The reach penalty is the main tribute to be paid for the capacity advantage of HOM formats. A 3 dB reach penalty reduces the transmission reach by 50% when going from one standard MQAM format to the next higher one ( $\Delta m_{DP} = 2$ ). These 3 dB steps express a significant granularity of transmission penalty. Transceivers operating with TDHM formats which reduce the step size of the modulation efficiency to e.g.  $\Delta m_{DP} = 0.5$  [48] are advantageous as they reduce at the same time the transmission penalty between the TDHM formats to 0.75 dB (16% transmission reach reduction) according to the slope of the reach penalty curve in Fig. 7.14 of 1.5 dB/bits/symbol.

A significant transmission reach advantage can be expected using probabilistically shaped HOM formats instead of standard HOM formats as probabilistically shaped constellations perform closer to the Shannon limit. In [80] a reach advantage of 35% has been demonstrated using a probabilistically shaped 64QAM format versus a standard 16QAM format.

The OSNR performance and reach penalty data presented in Fig. 7.14 are theoretical values and unfortunately real world OSNR values are coming with “implementation penalties” which are related to hardware limitations depending on constellation size and symbol rate. Minimum implementation penalties in the order of about 2 dB are observed for 32 GBd DP-QPSK, the penalties increase to about 3 dB for 32 GBd DP-16QAM, and they may reach more than 4 dB, as experimentally demonstrated for 21 GBd [81]. In general implementation penalties increase with the constellation size, however, this penalty can partly be overcome by coding gain improvements brought by empowered FEC.

### 7.3.3.3 Channel Grid for 400 Gbit/s Single Carrier and Dual Carrier FDM

In the following paragraph we will compare the 400 Gbit/s single with the dual-carrier option ( $2 \times 200$  Gbit/s) with respect to channel grid allocations at far (7.14) and near Nyquist (7.15) DWDM with bandwidth efficiencies of  $\eta \sim 0.64$  and  $\eta \sim 0.85$ , respectively. As in the previous section, we will include constellation sizes such as 128QAM and 256QAM as potential options for future short reach data center applications. Figure 7.15 illustrates the different channel spacing options of HOM formats including the corresponding symbol rates (blue bars), and the left and right parts of the figure correspond to 200 Gbit/s and 400 Gbit/s channel net rates (line rates in brackets), respectively. Green and red bars indicate the far and near Nyquist cases. The solid, colored bars show applications on the flexible grid with a frequency grid granularity of 12.5 GHz, according to the ITU-T standard [61]. The open colored bars show applications not covered by the flexible grid. We designate these as open grid applications as they do not match with the frequency grid granularity of 12.5 GHz and are not compliant with the ITU-T standard [61].

Due to the 2-fold higher symbol rate at 400 Gbit/s, the flexible grid granularity with 12.5 GHz appears to be sufficient up to high constellation sizes as a compar-

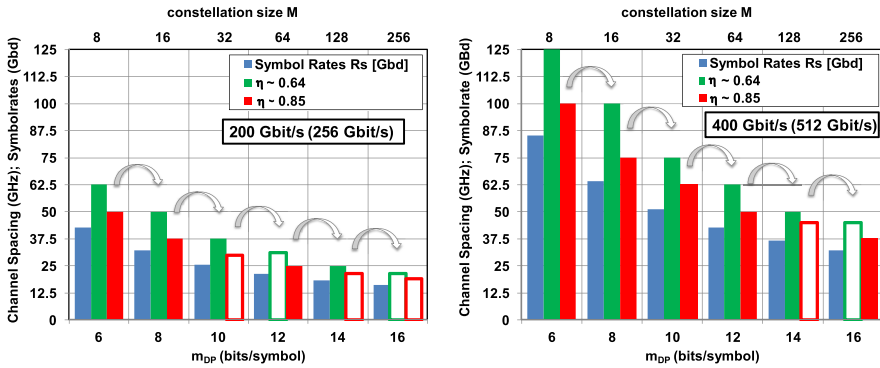


**Fig. 7.15** Channel spacings of HOM formats at 200 Gbit/s (*left*) and 400 Gbit/s (*right*), corresponding to  $\eta \sim 0.64$  and  $\eta \sim 0.86$  for flexible (*solid green and red bars*) and open grid allocation (*open green and red bars*)

ison of the solid and open bars in Fig. 7.15 demonstrates. At 200 Gbit/s, the flexible grid granularity is apparently rather insufficient as it is limited to DP-16QAM only. For example, DP-32QAM on a 37.5 GHz flexible grid ( $\eta \sim 0.64$ ) does not offer any spectral efficiency advantage compared to DP-16QAM for  $\eta \sim 0.86$ , as DP-32QAM with  $\eta \sim 0.86$  is on the open grid. If compliance with the flexible grid is requested, a further spectral efficiency gain would be provided only by DP-64QAM with  $\eta \sim 0.86$  on the 25 GHz flexible grid.

At 200 Gbit/s the use of hybrid modulation formats [48] would increase the spectral efficiency granularity and make it fit into the flexible grid granularity but for 400 Gbit/s hybrid modulation formats are not required in this respect. As already mentioned, the highest constellation sizes of the standard HOM formats, 128QAM and 256 QAM, are only suited for short reach (intra data center) applications where no flexible grid standard is targeted.

### 7.3.3.4 1 Tbit/s Few Sub-carriers FDM Options

In the past few years, significant research has been performed on the development of 1 Tbit/s transceivers, and the focus has mainly been on FDM. Like the first 100 Gbit/s and first 400 Gbit/s solutions, also future first 1 Tbit/s solution will be based upon FDM and the superchannel concept and the number of sub-carriers and the applied symbol rates will be determined by the available converter technologies.

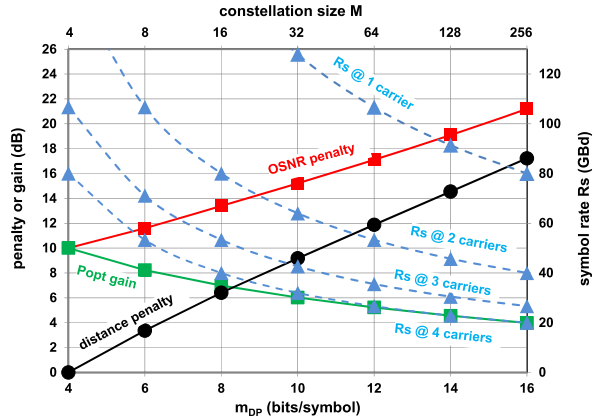
Table 7.8 shows single carrier and superchannel (FDM) options for the realization of 1 Tbit/s net rate and 1.28 Tbit/s line rate. As for 100 Gbit/s and 400 Gbit/s net rates, the true net rates include GE client rates and the line rates include 25% OH for SD-FEC. As in the case of Table 7.6 and Table 7.7, the color codes chosen for the symbol rates indicate the availability of the required digital converter technology within the next 5–10 years. Red (orange) indicates unlikely (likely) availability



**Table 7.8** 1 Tbit/s single carrier and superchannel (FDM) options: Symbol rates and constellation sizes for given number of sub-carriers. Colors at symbol rates indicate probability of converter availability within the next 5 to 10 years (see text)

Symbol rate (GBd)		43	53	71	40	53	80	32	64	128	53	107	46	91	40	80	36	71	32	64	
Net rate (Gbit/s)	Line rate (Gbit/s)	8																			
	const. Size M	16																			
1000	$m_{DP}$ (bits/symbol)	6																			
	no. of sub-carriers	5	4	3	4	3	2	4	2	1	2	1	2	1	2	1	2	1	2	1	2
		1280																			
		8																			
		32																			
		10																			
		12																			
		64																			
		128																			
		14																			
		128																			
		256																			
		16																			
		18																			
		512																			
		20																			

**Fig. 7.16** Reach penalty, OSNR penalty,  $P_{opt}$  gain and symbol rates per carrier versus constellation size for single and multiple carrier 1.28 Tbit/s options, penalty and gain values given relative to those of 128 Gbit/s DP-QPSK (32 GBd)



while DACs and ADCs required for the symbol rates highlighted in green are already available.

With current converter technology, which supports symbol rates of about 43 GBd, a 1 Tbit/s transceiver requires four sub-carriers e.g. together with DP-16QAM at 40 GBd or two sub-carriers e.g. together with DP-128QAM at 46 GBd, respectively. With future converter technologies which may support symbol rates up to  $\sim 70$  GBd or even 80 GBd, attractive two sub-carrier solutions can be based upon DP-64QAM with 53 GBd or on DP-32QAM with 64 GBd or even on DP-16QAM with 80 GBd.

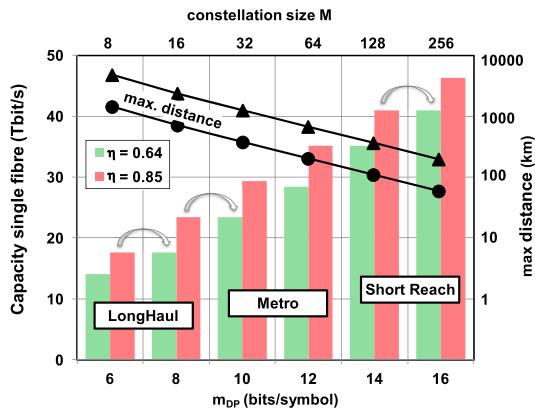
Similar to the 400 Gbit/s case shown in Fig. 7.14, Fig. 7.16 illustrates various 1 Tbit/s options (1.28 Tbit/s line rate) including: the development of OSNR penalty, fiber launch power ( $P_{opt}$ ) gain, and the reach penalty versus constellation size of the MQAM HOM formats with 128 Gbit/s DP-QPSK (32 GBd) taken as a reference. Figure 7.16 includes the symbol rates required for potential single carrier options and for two, three, and four sub-carrier FDM options.

The ten-fold higher bit rate compared to 128 Gbit/s DP-QPSK leads to 10 dB higher OSNR (penalty) at 1.28 Tbit/s DP-QPSK but comes together with 10 dB  $P_{opt}$  gain due to ten times broader spectral width. The resulting 0 dB reach penalty is in accordance with the case of  $10 \times 128$  Gbit/s DWDM as the spectral efficiency remains unchanged. If the spectral efficiency is increased by the constellation size, the OSNR penalty and the  $P_{opt}$  gain scale bit rate independently as in the case of 400 Gbit/s options shown in Fig. 7.14: the reach penalty increases in steps of 3 dB between the standards MQAM formats or with a slope of 1.5 dB/bits/symbol.

### 7.3.3.5 Transmission Reach Versus Capacity

Figure 7.17 summarizes the trade-off between maximum fiber capacities in the C-band for different constellation sizes of standard HOM formats and the maximum transmission reach over terrestrial SMF links with EDFA repeater and without dis-

**Fig. 7.17** Maximum single fiber capacities for dedicated application areas and maximum fiber (SMF) transmission distances (triangles: optimistic, points: pessimistic case) versus HOM formats for far Nyquist DWDM:  $\eta \sim 0.64$  (green bars) and near Nyquist DWDM:  $\eta \sim 0.85$  (red bars)



person compensation. Potential application areas are indicated. A distinction between flexible and open grid has not been made here. The capacity as well as the maximum transmission data are bit rate independent and hold for 200 Gbit/s, 400 Gbit/s or even 1 Tbit/s on a single carrier and are also valid for multiple carrier FDM solutions.

The maximum distance values designated as “pessimistic” correspond to the 1,500 km product performance of 112 Gbit/s DP-QPSK, data labeled “optimistic” correspond to 10,000 km research performance, and 14,000 km reach has been demonstrated with 128 Gbit/s DP-QPSK for EDFA repeated SMF transmission [82].

The advantage of pulse shaping together with HOM formats can be seen in Fig. 7.17 (similar to Fig. 7.12), as indicated by the arrows: by pulse shaping ( $\eta \sim 0.85$ , red bars) the same channel spacing, spectral efficiency, and capacity can be obtained as that achieved by the next higher HOM format without pulse shaping ( $\eta \sim 0.64$ , green bars), i.e., pulse shaping enables a modulation efficiency increase by 2 additional bits/symbol.

From today’s perspective the maximum single fiber capacities in the optical C-band feasible with standard HOM formats are  $\sim 24$  Tbit/s, 35 Tbit/s and 46 Tbit/s for long haul, Metro and short reach applications, respectively. The corresponding spectral efficiencies are 5.3, 8, and 10.7 bit/s/Hz achieved by DP-16QAM, DP-64QAM, and DP-256QAM, respectively. If the optical L-band is included, the available fiber bandwidths increase from 4.4 THz up to 11 THz [16], and the single fiber capacities can reach  $\sim 60$  Tbit/s, 87 Tbit/s, and 115 Tbit/s, respectively.

The application limitations visible in Fig. 7.17 can still be shifted significantly. For example, DP-64QAM may become an option for long-haul transmission by including (a) Raman amplification, so that the OSNR constraints and penalties of high constellation sizes become relaxed or (b) 3R regeneration, depending on the future cost development of coherent transceivers.

Recently probabilistically shaped DP-64QAM constellations [83] have been proposed for reach extensions. It has also been demonstrated [83], at same spectral efficiencies that probabilistically shaped DP-16QAM and DP-64QAM constellations

constellations perform with longer reach than regular DP-16QAM and DP-64QAM formats.

In submarine transmission configurations with gridless channel allocations, the channel spacing chosen and bandwidth efficiencies  $\eta$  are usually closer to Nyquist:  $0.85 < \eta < 1$ , enabled by the use of very low signal roll-off factors ( $< 0.1$ ) resulting in respective higher spectral efficiencies.

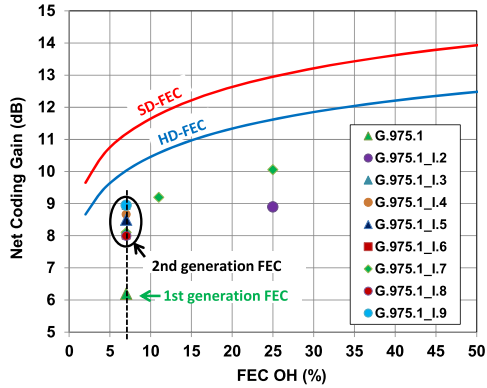
## 7.4 Forward Error Correction (FEC)

### 7.4.1 Hard Decision FEC

FEC has a long history in optical communication systems. It has been introduced in 2.5 Gbit/s OOK systems first and has become indispensable in today's coherent transmission systems. In 1995, the first FEC, using Reed-Solomon block codes, was applied in optical transport to bridge submarine transmission distances. In 10 Gbit/s NRZ terrestrial DWDM long-haul systems, the well-known Reed Solomon RS(255,239) block code was widely implemented as described by ITU-T recommendations G.975.1 [84] and G.709 [85] and was classified as first generation FEC. This RS(255,239) code requires an OH of 6.7% and corrects a pre-FEC-BER of  $2 \times 10^{-4}$  to post-FEC-BER  $< 10^{-15}$ , corresponding to a net coding gain (NCG) of 6.2 dB. During the development of 40 Gbit/s systems system engineers were looking for stronger FECs with higher NCG to compensate the 6 dB higher OSNR required by the new 40 Gbit/s bit rate systems compared to the installed 10 Gbit/s solutions. Most of the improved FEC schemes applied concatenated product codes [86] with e.g. inner-RS and outer-RS codes. More precisely, a bit stream is first encoded by an inner algorithmic code, code words are jointly interleaved, and after partitioning the product is encoded a second time by an outer algorithmic code. These codes achieve very good performance and low error floors with limited implementation complexity. The inner and outer codes of such schemes are often BCH (Bose-Chaudhuri-Hocquenghem) and/or RS codes. The advantage of BCH codes is that very efficient closed-form solutions exist for computing the error locations at the decoder [87]. Keeping the OH at 7%, the NCG could be improved significantly with these new FEC schemes, also denoted as enhanced FEC (E-FEC), summarized in G.975.1 [84]. These E-FEC codes have been classified as second generation FEC schemes, they provide NCG between  $\sim 8$  dB and  $\sim 9$  dB, and correct pre-FEC-BERs between  $10^{-3}$  and  $3.8 \times 10^{-3}$  to post-FEC-BER  $< 10^{-15}$ .

Figure 7.18 summarizes the NCG of different realized versions [84] of 2nd generation FEC including the NCG of 6.2 dB for the 1st generation FEC. Both generations are so-called hard decision FECs, as "0-1" decisions are performed. Figure 7.18 also includes the NCG of further implemented HD-FEC schemes with 11% and 25% FEC OH [84].

**Fig. 7.18** Net coding gain (NCG) of 1st and 2nd generation HD-FEC codes and theoretical limit of HD-FEC and SD-FEC schemes versus FEC OH



### 7.4.2 Soft Decision FEC

Since the first implementations of 100G transponders which used second generation HD-FEC, there has been intensive research to develop even more powerful FEC codes with NCG beyond 10 dB by soft-decision [88, 89] but also allowing higher OH than 7% only. Soft-decision means that no “0-1” decisions are made prior to FEC decoding but all information coming from the DSP is exploited. If hard “0-1” decisions are made at an early stage of signal processing, information is lost which could otherwise be used to improve the FEC performance.

Figure 7.18 includes the theoretical limit of NCG for HD-FEC and SD-FEC depending on the FEC OH, which has been described by Shannon’s second theorem [38]. A performance gain between 1 and 1.5 dB is observed for SD-FEC compared to HD-FEC in the range between 2% and 50% of OH, respectively. For example, the ultimate NCG limit for SD-FEC with 25% OH is 12.9 dB which we will consider in this chapter for the comparison of HOM formats.

SD-FEC schemes are designated as third generation FEC, they are significantly more complex and consume significantly more power than the first and second generation HD-FEC schemes, at the encoder as well as at the decoder side but they also allow higher flexibility. In general, for HD-FEC less information needs to be transferred between the receiver DSP and the FEC decoder. In the case of SD-FEC the data flow is significantly higher and a fast interface is required between SD-FEC and the coherent receiver DSP, thus both have to be implemented together in one ASIC. Since the introduction of 35 nm CMOS technology this became feasible and has been realized with reasonable power consumption. Second generation 100 Gbit/s transponders already include SD-FEC with ~25% OH and a small amount (typically ~3%) of HD-FEC to correct for error-floors [90].

Two competing classes of SD-FEC are currently investigated for 100 Gbit/s systems and beyond. The first class uses block turbo codes (BTC) and is in principle an extension of second generation concatenated codes and applies so-called iterative soft-decision decoding [91]. BTC decoders are highly parallelizable while keeping the internal decoder data flow low, they converge rather fast and require a small

number of decoding iterations only. The main disadvantage of these codes is their relatively large block length leading to larger delays. Further disadvantages include inflexibility with respect to varying frame sizes and overheads.

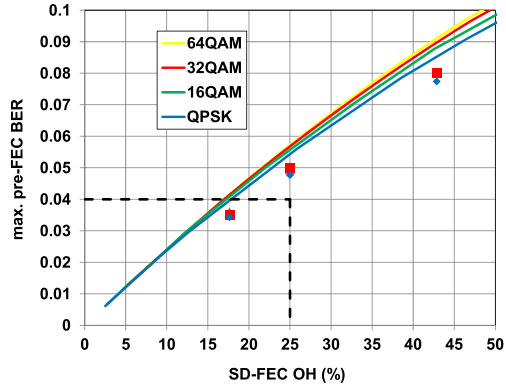
The second class are low-density parity-check (LDPC) codes applying maximum a posteriori (MAP) soft-decision decoding. LDPC codes have been invented in 1963 [92] and were rediscovered in the 90ies of the last century and are applied in wireless (WLAN, IEEE 802.11, DVB-S2) and powerline communication (IEEE 1901) and 10G Ethernet (IEEE 802.3). The first LDPC code implemented in optics was an HD-FEC scheme included in the second generation FEC scheme in G.975.1. Latest developments of LDPC codes for future optical communication systems are given in [93]. Compared to BTC schemes LDPC codes have relatively simple algorithms allowing a high degree of flexibility as there exists no common design rule. Various algorithms have been proposed for 100G and beyond systems with advantages and disadvantages. The target design is a code that yields high coding gain, fast convergence and that is implementable in the considered CMOS technology with reasonable power consumption. LDPC codes usually suffer from an error floor at BERs between  $10^{-6}$  and  $10^{-10}$ . Therefore, modern FEC systems are typically constructed using an SD-LDPC inner code which reduces the BER to a level of  $10^{-3}$  to  $10^{-5}$  and an HD outer code which pushes the post FEC-BER to levels well below  $10^{-12}$ , as proposed in [94]. With the latest generation of LPCD codes floorless error correction [95] is achieved so that no additional HD-FEC is required.

For the application of HOM formats which come along with increasing OSNR sensitivity constraints, improved FEC performance becomes more and more essential. One option to meet this challenge is to trade off part of the modulation efficiency of HOM formats against higher overhead and thus for stronger SD-FEC so that the higher OSNR demands can at least partially be relieved.

The curves in Fig. 7.19 show the theoretically maximum correctable pre-FEC BER (pre-FEC threshold) as a function of OH for SD-FEC for four examples of HOM formats. The use of pre-FEC threshold as theoretical limit in the case of SD-FEC has been questioned [44] and the generalized mutual information has been claimed to be a better predictor. However, at an SD-FEC OH of 25% under consideration here it was also pointed out in [44] that the differences for the pre-FEC in order to obtain a required post-FEC are very small and become significant only for much higher OH.

Realistically achievable values of maximum pre-FEC BERs with SD-FEC were confirmed for different OH and different HOM formats as illustrated by the points in Fig. 7.19. These maximum pre-FEC BER values were obtained for a class of spatially coupled LDPC codes [96], currently one of the best known schemes for SD-FEC. This class of codes has been successfully verified in various transmission experiments, e.g., for high spectral-efficiency ultra long-haul submarine transmission [97]. It can be seen that this class of codes allows one to operate close to the theoretical limits, shown by the curves in Fig. 7.19 where a dependency on HOM formats can be observed. These theoretical limits of pre-FEC BER at 25% OH appear to be in the range between 0.054 and 0.057 for QPSK and 64QAM, respectively. Extrapolation to 1024QAM suggests that the maximum pre-FEC BER should

**Fig. 7.19** Maximum tolerable pre-FEC BER vs. SD-FEC overhead for QPSK, 16QAM and 32QAM, curves show theoretical performance, *points* show simulated SD-FEC decoder performance



not exceed 0.059 at 25% OH. The use of a single common pre-FEC BER of 0.04 at 25% OH for the comparison of HOM formats appears pessimistic according to Fig. 7.19 and therefore we conclude that the performance of very high constellation sizes appears to be slightly underestimated compared to low constellation sizes.

## 7.5 Digital Signal Processing

### 7.5.1 Transmitter Digital Signal Processing

If DACs and DSPs are included in a transmitter, a single transceiver with enormous flexibility is obtained. The DSP and DAC allow for the generation of HOM formats together with spectral pre-shaping which becomes a mandatory feature for the optimization of the spectral efficiency of near Nyquist shaped flat top signal spectra. In addition, the modulation format of the transceiver can be dynamically changed on the fly by the DSP if the routed signal path is changed and transmission impairments vary. Besides standard HOM, modulation formats with different FEC codes can also be included [98]. Furthermore, hybrid HOM formats like time domain hybrid modulation formats can be included to further increase the granularity of standard HOM [47, 48], to better adapt for targeted transmission distances. Finally, a variety of equalization functions can be addressed in addition to spectral pre-shaping (pulse shaping): (a) equalization of the frequency modulation response given by the concatenation of the DAC, the driver, and the modulator, (b) compensation of the sinusoidal modulation characteristics of the MZM, (c) dispersion pre-compensation, (d) SPM pre-compensation etc. Thus software defined transceivers can be implemented if DACs and transmitter DSP are included.

As reported in Sect. 7.3.1.5, high speed DACs implemented in ASICs for optical transceivers have a limited available resolution, determined by the ENOB, typically between 4 and 6 bits, and the degree of realizable equalization functionality is determined by the target constellation size. Apparently there is a trade-off between

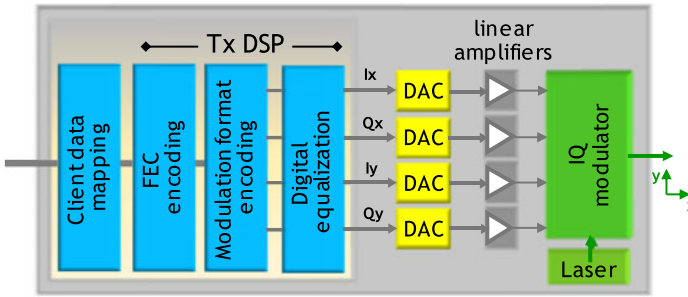


**Fig. 7.20** Transmitter building blocks

the desired constellation size and the realizable equalization [99]. For example, as shown in Table 7.3, if DP-64QAM is targeted with DACs and if an ENOB of 5 bits is assumed, there are two bits available for equalization functions. In [100] it has been estimated that pulse shaping requires 1 bit in effective resolution, and 1 additional bit is required for equalization of the frequency modulation response, as a consequence, the application of 64QAM is possible in that example.

Figure 7.20 shows the main transmitter building blocks, consisting of Tx DSP and four DACs which convert the digital representations of the four tributaries  $I_x$ ,  $Q_x$ ,  $I_y$  and  $Q_y$  to multi-level analogue signals. These are subsequently amplified by linear amplifiers and launched to a DP-IQ modulator. In the following discussion we will restrict ourselves to the Tx DSP block consisting of client data mapping, FEC encoding, modulation format encoding, and digital equalization.

*Data Mapping:* At the input of a transceiver so-called client signals arrive. Since the GE Ethernet and optical transport hierarchy met with 100GE and 100 Gbit/s (OTU-4) standards in 2010, the client data are mostly GE based. Including synchronization and data skewing, these data are mapped onto the four tributaries  $I_x$ ,  $Q_x$ ,  $I_y$ , and  $Q_y$ , where  $I$  and  $Q$  are the in-phase ( $I$ ) and quadrature ( $Q$ ) components of the signal in  $x$  and  $y$  polarization, respectively.

*FEC Encoding* includes encoding of data by HD-FEC or by SD-FEC. If only SD-FEC is used, the applied LDPC code must allow for error floor free performance at the receiver side. More details on FEC were summarized in Sect. 7.4.2.

*Modulation Encoding* includes the mapping of the FEC encoded bits onto the desired HOM format. Depending on the available resolution, modulation encoding potentially includes the equalization of the MZM sinusoidal characteristics by adapting the digital representation of the amplitude and phase levels to the symbol constellations.

*Digital Equalization* at the transmitter side uses fixed static none adaptive equalizers usually implemented by time-domain FIR filters. The equalization includes the equalizing function shown above. The equalization of the frequency response of DAC, driver, and modulator is performed with the target of achieving a flat top output spectrum which is achieved by signal pulse shaping.



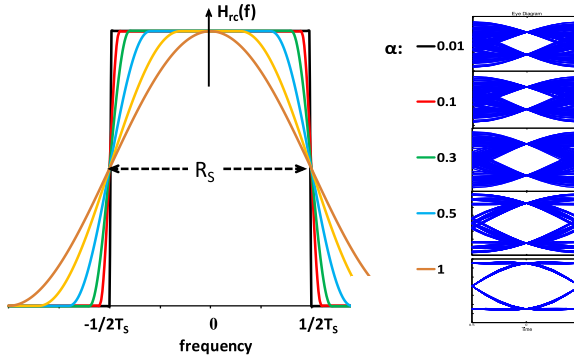


Fig. 7.21 Raised-cosine filter response (spectrum) and eye-diagrams for various roll-off factors  $\alpha$

### 7.5.1.1 Spectral Pre-shaping

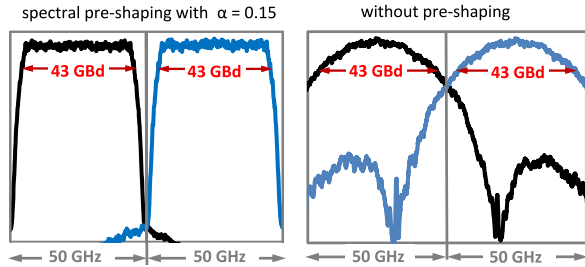
The key motivations for spectral pre-shaping or Nyquist pulse shaping are (a) raising the spectral efficiency in order to maximize the fiber capacity (see Sect. 7.3.2) by appropriate control of the transmitter signal spectrum, (b) minimizing intersymbol interferences (ISI) and (c) increasing the nonlinear tolerance of the transmitted signal. A widely used filter function is the raised cosine (rc) function  $H_{rc}(f)$  given by (7.19)

$$H_{rc}(f) \begin{cases} 1; & |f| < \frac{1-\alpha}{2T_S} \\ \cos^2\left(\frac{\pi T_S}{2\alpha} \left(|f| - \frac{1-\alpha}{2T_S}\right)\right); & \frac{1-\alpha}{2T_S} < |f| < \frac{1+\alpha}{2T_S} \\ 0; & \text{else} \end{cases} \quad (7.19)$$

and filtering is typically implemented in such a way that the filtering is shared between the transmitter and the receiver. The corresponding filter function at both sides is a root raised cosine filter  $H_{rrc}(f)$  with  $T_S = 1/R_S$  ( $R_S =$  symbol rate) and  $\alpha$  as the roll-off factor. Figure 7.21 represents the rc filter function (spectrum) with variable roll-off factors between 0.01 and 1. The function  $H_{rc}(f)$  acts as an ideal low pass filter for the case of  $\alpha = 0$  and it eliminates all undesired out of band signal contributions. The full width at half maximum (FWHM) of the spectrum corresponds to the symbol rate  $R_S$  for all roll-off factor cases. Figure 7.21 includes simulated binary eye-diagrams with rc modulation and the corresponding roll-off factor. As a compromise between remaining eye-opening and spectral properties, actually implemented roll-off factors are usually between 0.1 and 0.2 for terrestrial transmission applications.

Figure 7.22 shows a comparison of the spectral characteristics of two 43 GBd (DP-16QAM modulated) signals on the 50 GHz grid with bandwidth efficiency of  $\eta \sim 0.85$  (near Nyquist DWDM), one with and the other without spectral pre-shaping. Spectral pre-shaping (left channel pair) provides significantly better channel separation and significantly lower linear crosstalk than what can be obtained without pre-shaping (right channel pair), measured crosstalk penalties are less than

**Fig. 7.22** Spectral characteristics of 43 GBd DP-16QAM signal pairs for 50 GHz channel spacing; *left side*: with spectral pre-shaping with  $H_{rc}(f)$  and  $\alpha = 0.15$ , *right side*: no spectral pre-shaping



0.2 dB and more than 2 dB, respectively. If targeting without pre-shaping together with less than 0.2 dB cross talk penalty between neighboring channels, the channel spacing must be higher and the spectral efficiency becomes 30 to 40% lower. In addition, higher nonlinear tolerance of pre-shaped signals has been demonstrated in [101].

### 7.5.2 Receiver Digital Signal Processing

In general there are two different approaches for the receiver signal processing: either signal processing using training sequences or signal processing using full blind adaptation; in this section we will concentrate on full blind adaptation. Figure 7.23 shows the building blocks of the coherent receiver. The four analogue tributaries ( $I_x$ ,  $Q_x$ ,  $I_y$ , and  $Q_y$ ) received from the phase and polarization diversity receiver frontend are linearly amplified and digitized by four high speed ADCs and fed to the receiver DSP. The DSP comprises the following stages: timing recovery, frontend corrections, dispersion equalizer, polarization recovery, carrier frequency recovery, and phase recovery. After passing these blocks the symbols are recovered and the HOM has to be decoded. Finally the FEC has to be decoded and the signals have to be mapped to client rates.

*Timing Recovery* is the first DSP building block to resample/synchronize the oversampling ratio of the signal to a 2-fold ratio. In favor of that the phase of the received signal has to be estimated using the Gardner timing recovery [102] or the square timing recovery [103]. Due to operating the system in the digital domain

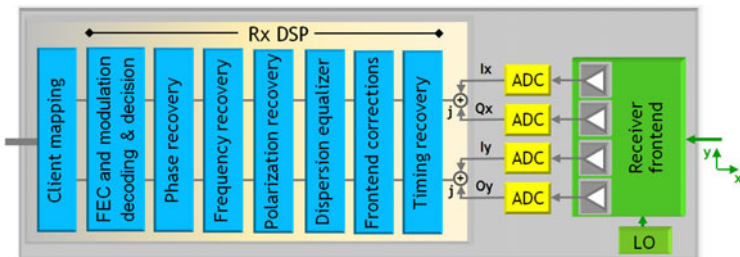


**Fig. 7.23** Coherent receiver building blocks

without closed feedback loop a full synchronous sampling is impossible. Therefore any phase offset has to be compensated by an interpolation filter. In order to minimize the offset the phase estimation may be used to adjust the ADC's sampling frequency.

*Frontend Corrections* are applied to compensate for quadrature imbalances that may originate from imperfect phase reception of the optical  $90^\circ$  hybrid. Quadrature imbalance compensation is well known in wireless communication and has been proposed to be used in optical communications as well [104]. A detailed example of  $I$ - $Q$  imbalance compensation is reported in [105] by measuring and minimizing the cross correlation between the in-phase ( $I$ ) and quadrature ( $Q$ ) components of the received signal, employing a feedback structure. The  $I$ - $Q$  output results from a linear combination of the received  $I$ - $Q$  signals.

*Chromatic Dispersion Compensation* is performed in two steps: at first by static dispersion equalization with slow update rates for compensation of high chromatic dispersion values while fast residual dispersion compensation by an adaptive equalization is performed in the following polarization recovery part. The target filter function is a simple all pass filter for the compensation of differential group delay. The number of required filter taps for compensation of the CD increases linearly with the dispersion and therefore linearly with fiber length.

A static equalizer [106, 107] can be implemented either in the time [108] or in the frequency domain [109] with different degrees of complexity which rises proportional to  $N$  or  $\log_2 N$ , respectively, where  $N$  is the number of filter taps. The number of taps is typically large and suitable for the compensation of the CD of a few 1000 km of SMF. Therefore an implementation of the CD filter in the frequency domain is advantageous. The tap weights are complex numbers in the time domain implementation, while the tap weights in the frequency domain implementation are complex numbers with modulus 1.

*Polarization Recovery including PMD Compensation* is typically performed in a  $2 \times 2$  MIMO configuration [107]. Also designated as a butterfly structure including four independent adaptive filters partitioned into three parts: The actual FIR filter bank, error estimation, and calculation of updated filter coefficients [110].

The actual filter bank consists of simple FIR filters. At this point in the processing chain the carrier frequency and the phase are not yet estimated nor compensated. At the polarization recovery output the constellations are still rotating in the complex plain. Therefore decision directed adaptation schemes are more difficult to implement for polarization recovery including PMD compensation.

A very popular blind adaptation scheme for error estimation is the constant modulus algorithm (CMA) [111] which optimizes deviations of the amplitude of the equalized signal from a desired fixed value. In the case of rotating symbols the unit circle is used as adaptation target. The standard CMA is optimally suited for purely PSK modulated signals, including QPSK, with all symbols on a ring corresponding to constant intensity (constant modulus). For HOM formats multi-modulus algorithms (MMA) have been proposed [112] although the standard CMA is applicable for HOMs too. The most widely used implementation for the calculation of filter coefficient updates is the least-mean-squares algorithm [113]. The idea of the LMS

algorithm is to estimate the gradient of the error by partial derivatives of the mean squared error with respect to the filter coefficients. The exact formulation of this algorithm and a comparison with a decision feedback structure can be found for instance in [114]. The update of the filter coefficients and the resulting convergence speed must be fast enough for the compensation of the fastest expected polarization changes. On the other hand the filters must also be long enough to simultaneously compensate for the maximum expected polarization dependent delays. These are determined by the maximum differential group delay (DGD) expected for the transmission link at the end of which the transceiver is expected to operate. The filter acts as a channel equalizer, too. If  $H_{rrc}(f)$  pulses are applied with very low roll-off factors, the long impulse response of the channel equalizer may dominate the filter length. At the filter input oversampled data are applied, and at the output baud rate sampled data are required for further processing.

*Carrier Frequency Recovery or Frequency Offset Compensation:* The frequency offset between the Tx laser and the LO determines the rotation frequency of the whole constellation in the  $I-Q$  plane and can be estimated in the frequency domain. A common method is using the  $M$ th power nonlinearity in order to find the frequency with the maximum power in the Fourier transform of the residual signal after the modulation has been removed [115]. The estimated carrier frequency is used to downconvert the signal into the baseband by one complex multiplication.

*Carrier Phase Recovery* is required to finally remove phase differences or phase walk-off between the Tx and LO carriers by either using a joint-polarization approach [116], feed-forward  $M$ th power phase estimation [117] or a Viterbi-Viterbi algorithm [118]. More details can be found in [119]. After application of the  $M$ th power of the symbols the modulation is removed, the carrier phase can be estimated, and one more complex multiplication finally compensates the carrier phase. At the output of the carrier phase recovery the symbols are regenerated completely.

*Modulation Decoding and FEC Decoding:* The modulation has to be decoded depending on the Tx encoding scheme in order to regenerate the binary data, and these data are finally FEC decoded according to the applied FEC scheme.

## 7.6 Data Converters (DAC and ADC)

Enabled by the progress on integration of Si technology, first high speed DAC and ADC technologies have been implemented in 2005 in 10 Gbit/s direct detection systems [120, 121] supporting sampling rates of  $\sim 20$  GSamples/s, and the target was the compensation of chromatic dispersion in the electronic domain by pre-compensation or by post-compensation, respectively. Initially coherent 40G and 100G transponders required ADCs at the receiver only but DACs at the transmitter side became the key enabler for HOM formats and DACs enabled flexible adaptation of formats, equalization of components frequency response and spectral pre-shaping in order to optimize spectral efficiencies.

Several DAC and ADC concepts or architectures are known today, and their suitability for a specific application is determined by: physical size, power consumption,

resolution, speed, accuracy and cost. While the architectures of high-speed DACs and high speed ADCs are significantly different, the common attributes of both are: effective resolution, linearity, maximum sampling rate, total harmonic distortions, noise floor, clock speed, jitter, bandwidth, suitability for integration with the DSP and power dissipation.

The realization of data converters for first generation and current state-of-the-art coherent transceivers is summarized in Sect. 7.7.3 on ASIC technologies.

### 7.6.1 Digital-to-Analogue Converters

In this section we will describe the main parameters which characterize DACs and summarize the principles of typical high speed DAC architectures that have been realized for optical communication. We will focus here on high speed DACs with a minimum resolution of 6 bits that can be applied for ASICs including transmitter DSP in commercial transceiver implementations.

#### 7.6.1.1 DAC Performance Parameters

DACs are characterized by static and dynamic parameters as described in detail below. Dynamic performance measurements are based on spectral analysis: The DAC is loaded with a digital image of a single or multi-tone sine-wave signal with frequency smaller than the Nyquist frequency (half the maximum sampling frequency of the DAC) and the DAC's output spectrum is measured with a spectrum analyzer.

Two static parameters characterize the DAC's linearity: the differential non-linearity (DNL) and the integral nonlinearity (INL). Both parameters are measures of the linearity of the level transitions of the converter and both affect the converter's quantization performance, so that due to the effects of DNL and INL the static effective number of bits is already less than the theoretically expected resolution. The basic dynamic DAC parameters are: the 3 dB electrical bandwidth, the maximum sampling rate, the signal-to-noise ratio without harmonics, the signal to total harmonic distortion ratio (THD), the signal to noise and distortion ratio (SINAD), the spurious free dynamic range, and finally the dynamic number of bits, as explained below.

*DAC Resolution:* The resolution of a DAC is determined by the number ( $n$ ) of bits of possible output levels ( $2^n$ ) the DAC is designed to reproduce. For instance, a 1 bit DAC is designed to reproduce only 2 ( $2^1$ ) levels while an 8 bit DAC is designed for 256 ( $2^8$ ) levels. This designed resolution corresponds to a theoretical resolution, and in reality the quantization of a signal with higher resolution leads to an unavoidable quantization error [99].

*Maximum Sampling Rate:* A measurement of the maximum speed at which the DAC's circuitry can operate and still produce the correct analogue output.

*Signal-to-Noise-and-Distortion Ratio (SINAD or SNDR)*: SINAD is a good indication of the overall dynamic performance of a DAC because it includes all components which contribute to noise and distortion. Signal-to-noise-and-distortion (SINAD, or  $S/(N + D)$ ) is the ratio of the signal amplitude to all other spectral components, including noise and harmonics while SNR and THD are the signal to noise and signal to distortion ratios, respectively.

$$SINAD = 20 \log \left( \frac{S}{N + D} \right) = 20 \log \sqrt{(10^{-SNR/20})^2 + (10^{-THD/20})^2} \quad (7.20)$$

*Effective Number of Bits (ENOB)*: A measure of the actual resolution of a DAC is ENOB which is generally smaller than the theoretical or designed resolution of a DAC. ENOB is frequency dependent and usually decreases towards the highest sampled frequency. ENOB (7.21) is calculated from SINAD measurements using the relationship for the theoretical SNR of an ideal  $n$ -bit DAC or ADC:  $SNR = 6.02n + 1.76$  dB [122]. The equation is solved for  $n$ , and the value of SINAD is substituted for SNR:

$$ENOB = \frac{SINAD \text{ (dB)} - 1.76}{6.02} \quad (7.21)$$

*Spurious Free Dynamic Range (SFDR)*: The SFDR is the ratio of the rms value of the signal to the rms value of the worst spurious signal regardless of where it occurs in the frequency spectrum. The worst spurious signal may or may not be a harmonic of the original signal. SFDR is an important specification in communication systems because it represents the smallest value of signal that can be distinguished from a large interfering signal (blocker). SFDR can be specified with respect to full-scale (dBFS) or with respect to the actual signal amplitude (dBc).

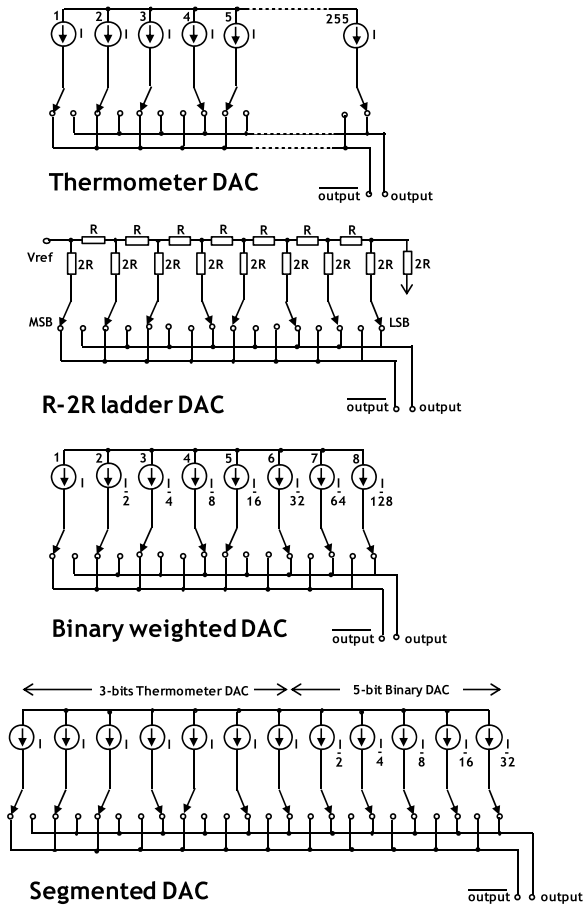
### 7.6.1.2 DAC Architectures

During the past 10 years four different DAC concepts have been considered, all based on current steering logic and differential analogue output [122], thermometer-coded, R-2R resistor ladder, binary weighted, or segmented DAC. Figure 7.24 shows the architectures of these DACs, all in an 8-bit theoretical resolution configuration.

*Thermometer-Coded DAC (TMC-DAC)*: The TMC-DAC, or “fully decoded DAC”, in a version with active current sources, contains  $2^n - 1$  identical current-source segments, one segment for each possible value of DAC output, i.e. 257 elements in the case of an 8 bit DAC. Thermometer-coded DACs require decoder logic and are very large but are fast and ensure very high monotonicity.

*R-2R Resistor Ladder DAC (R-2R-DAC)*: The R-2R-DAC is based on an R and 2R resistor ladder network with two resistors with ratio of 2:1 per stage. An  $n$ -bit DAC requires  $2n$  resistors. In this architecture, all stages have identical devices and matched resistors which can be trimmed easily. The output impedance of the DAC is equal to R (relatively low). A distinct advantage is that only a 2:1 resistor ratio

**Fig. 7.24** Principles of various DACs all 8-bit resolution



is required regardless of the resolution. This architecture requires no decoding logic but dissipates significant power (mainly in the internal resistors), and high resolution converters perform slowly due to increasingly large RC-constants for each added R-2R link.

**Binary-Weighted DAC (BW-DAC):** A BW-DAC with  $n$ -bit resolution contains  $n$  individual current sources. These precise currents are weighted with powers of two ( $1 : 2 : 4 : 8 : \dots : 2^{n-1}$ ) and sum up to the correct output value. This is a very fast conversion method but it suffers from poor accuracy because of the high precision required for each individual voltage or current. Such high-precision components are expensive, and therefore this type of converter is usually limited to 8-bit resolution or less, it dissipates less power than R-2R-DACs, requires smaller area, however, glitching (transients) is an issue.

**Segmented DAC (SEG-DAC):** An SEG-DAC or hybrid DAC uses combinations of the techniques explained above in a single converter. If a DAC with a specific performance is required, a single architecture is often not ideal, therefore most DACs

**Table 7.9** Advantages and disadvantages of various DAC concepts

DAC concept	Advantages	Disadvantages
TMC-DAC	identical stages, monotonicity	$2n$ current sources, decoding logic, large area
R-2R-DAC	only 2 resistor values, identical stages, no decoding logic	power dissipation of resistors
BW-DAC	$n$ current sources, no decoding logic	large current ratios
SEG-DAC	overshoot reduction	additional logic

are of segmented type in response to the challenge to achieve low cost together with high speed and high resolution in one device. A segmented DAC is divided into two sub-DACs including e.g. one thermometer-coded DAC for the most significant bits (MSBs) and one binary weighted DAC for the least significant bits (LSBs). Segmentation allows higher-resolution DAC implementations at the cost of additional logic. Finally, transients are also reduced significantly by this method.

Table 7.9 summarizes the advantages and disadvantages of the DAC concepts.

## 7.6.2 Analogue-to-Digital Converters

Fast ADCs followed by DSP are the key concept and enabler of coherent receivers. In this section we will discuss the main parameters characterizing ADCs and summarize the architectures of typical high speed ADCs [123] applied in optical communication.

### 7.6.2.1 ADC Performance Parameters

ADCs have similar static and dynamic parameters as DACs and dynamic characterization is also performed by spectral analysis [124]. If an ADC operates at a sampling rate greater than twice the bandwidth of the signal, then a reliable digital reproduction of an analogue signal is possible according to the Nyquist sampling theorem, provided the ADC can be considered ideal and quantization errors can be neglected. In contrast to DACs, ADCs require sampling and hold of the analogue input signal as ADCs cannot perform an instantaneous conversion. The input value must be held constant during the time in which the converter performs a conversion. An input circuit called a sample-and-hold or a sample-and-hold amplifier (SHA) performs this task, e.g. a capacitor plus a gate. SHAs are affected by noise, distortions, and aperture jitter.

The static parameters DNL and the INL characterize the ADC linearity. The dynamic parameters are: 3 dB electrical bandwidth, signal to noise ratio and distortion ratio, sampling rate, aliasing, jitter, and the effective number of bits.

*ADC Resolution:* The resolution of  $n$  bits of an ADC indicates the number of  $2^n$  discrete values or voltage levels it can produce. The minimum change in voltage



required to guarantee a change in the output code level is called the least significant bit (LSB) voltage, corresponding to the resolution of the ADC according to (7.22)

$$LSB = E_{FSR}/2^n \quad (7.22)$$

where  $n$  is the ADC's resolution in bits and  $E_{FSR}$  is the full scale voltage range (also called span).

*Sampling Rate of ADC:* The sampling rate (GSamples/s) of ADCs defines the rate at which digital values are sampled from the analogue signal.

*Effective Number of Bits (ENOB):* Similar to the case of DACs, the ADC can resolve a signal to a certain number of bits of resolution only (ENOB, see (7.21)) and the resolution of the ADC is limited mainly by the SNR of the digitized signal. One effective bit of resolution changes the SNR by a factor of  $2^1$  or by 6 dB in voltage. TIAs in front of an ADC introduce further noise and may further reduce the ENOB. A non-ideal sampling clock or aperture including unavoidable clock jitter will result in additional recorded noise that will also reduce the ENOB. As for ADCs the ENOB of DACs is frequency dependent as illustrated e.g. by the so-called Walden plot [125] which shows the ENOB versus ADC input frequency.

*Aperture Jitter* is phase noise of the sampling clock. Care must be taken to minimize this sampling jitter on the sampling clock in the sample-and-hold circuit. Aperture jitter limits the sampling rate and also the ENOB.

*Signal to Noise and Distortion Ratio (SINAD or SNDR):* If aperture jitter is the only determining factor, the SNDR [126] is given by

$$SNDR \text{ (dB)} = -20 \log(2\pi f t_j) \quad (7.23)$$

where  $f$  is the analogue input frequency and  $t_j$  is the rms aperture jitter of the ADC.

*Signal-to-Quantization-Noise Ratio (SQNR):* Quantization error is the noise introduced by “quantization” in an ideal ADC. The resolution determines the magnitude of the quantization error and therefore determines the maximum possible average signal to noise ratio. For an ideal ADC the SQNR can be calculated by:

$$SQNR \text{ (dB)} = 20 \log 2^n \sim 6.02n \quad (7.24)$$

where  $n$  is the number of quantization bits or the bit resolution. For example, an 8-bit ADC has a maximum signal-to-noise ratio of  $6.02 \times 8 = 48.16$  dB, and thus the quantization error is 48.16 dB below the maximum level. Quantization error is distributed from DC to the Nyquist frequency. If part of the ADC's bandwidth is not used, as in the case of oversampling, some of the quantization error will fall out of band which effectively improves the SQNR. In an oversampled system, noise shaping can be used to further increase the SQNR by forcing more quantization error out of the band.

*Aliasing:* If sampling above the Nyquist rate (i.e. more than twice the highest frequency) is possible, then all frequencies in the signal can be reconstructed (oversampling). Sampled frequencies above half the Nyquist rate are incorrectly detected compared to lower frequencies, and this process is designated as aliasing. In order

to avoid aliasing, the input of an ADC can be low-pass filtered which removes frequencies above half the sampling rate. Such a filter is called an anti-aliasing filter and is essential for ADC systems that are designed for analogue signals with higher frequency content.

### 7.6.2.2 ADC Architectures

As already mentioned, ADC and DAC architectures are significantly different and ADCs can be implemented in various ways with different pros and cons. The most popular high speed ADCs for DSP applications are flash-, successive approximation register-, pipelined-, ripple-, and time-interleaved ADC architectures. Various concepts of ADCs that have been considered and realized for optical coherent receivers will be summarized in the following section. The corresponding ADC architectures are shown in Fig. 7.25, all in 8-bit theoretical resolution configuration.

*Flash ADC (F-ADC):* Direct-conversion or parallel or flash ADCs have a large number ( $2^n - 1$ ) of comparators which sample the input signal in parallel. The comparators are separated by resistors which reduce the reference voltages by 1 LSB voltage between comparators. Each comparator is followed by a logic circuit which generates a code for each voltage range. This kind of a direct conversion is very fast, capable to operate at Gb/s sampling rates, but has limited resolution of  $\sim 8$  bits or fewer, due to the high number of comparators and resistors needed, e.g. a 8-bit flash ADC requires  $2^8 - 1 = 255$  comparators. ADCs of this type have a large die size and high power dissipation.

*Successive Approximation Register ADC (SAR-ADC):* An SAR-ADC executes conversion on demand based on SHAs and comparators. The approximation is stored in a successive approximation register after each comparator step, fed back to a DAC, and compared again until the desired resolution is reached. The overall accuracy and linearity is determined by the DAC. Bit by bit, the SAR-ADC is successively narrowing the range of input voltages from the MSB voltage down to the LSB voltage. An  $n$ -bit conversion takes  $n$  steps. This serial operating procedure of an SAR-ADC limits its operating speed.

*Pipeline ADC (PL-ADC):* PL-ADCs or sub-ranging ADCs combine the advantages of SAR- and flash-ADCs. After the SHA a first flash ADC works on 4 bits and results in a coarse conversion, the difference between that value and the input signal is determined with a DAC (4 bit resolution) and then converted finer by a further flash-ADC. A pipeline ADC enables higher resolution and has lower power consumption than a pure flash ADC.

*Serial Ripple ADC (SR-ADC):* SR-ADCs are converting with a cascade of one stage per bit. Each of the  $n$  stages has a bit output and a residue output. The residue output of one stage is the input to the following stage. Finally, the LSB is detected with a single comparator as shown in Fig. 7.25. This architecture is slightly slower than the flash topology. It is a simple architecture since the number of amplifiers and flip-flops is equal to the resolution. However, propagation delay through each stage is critical.

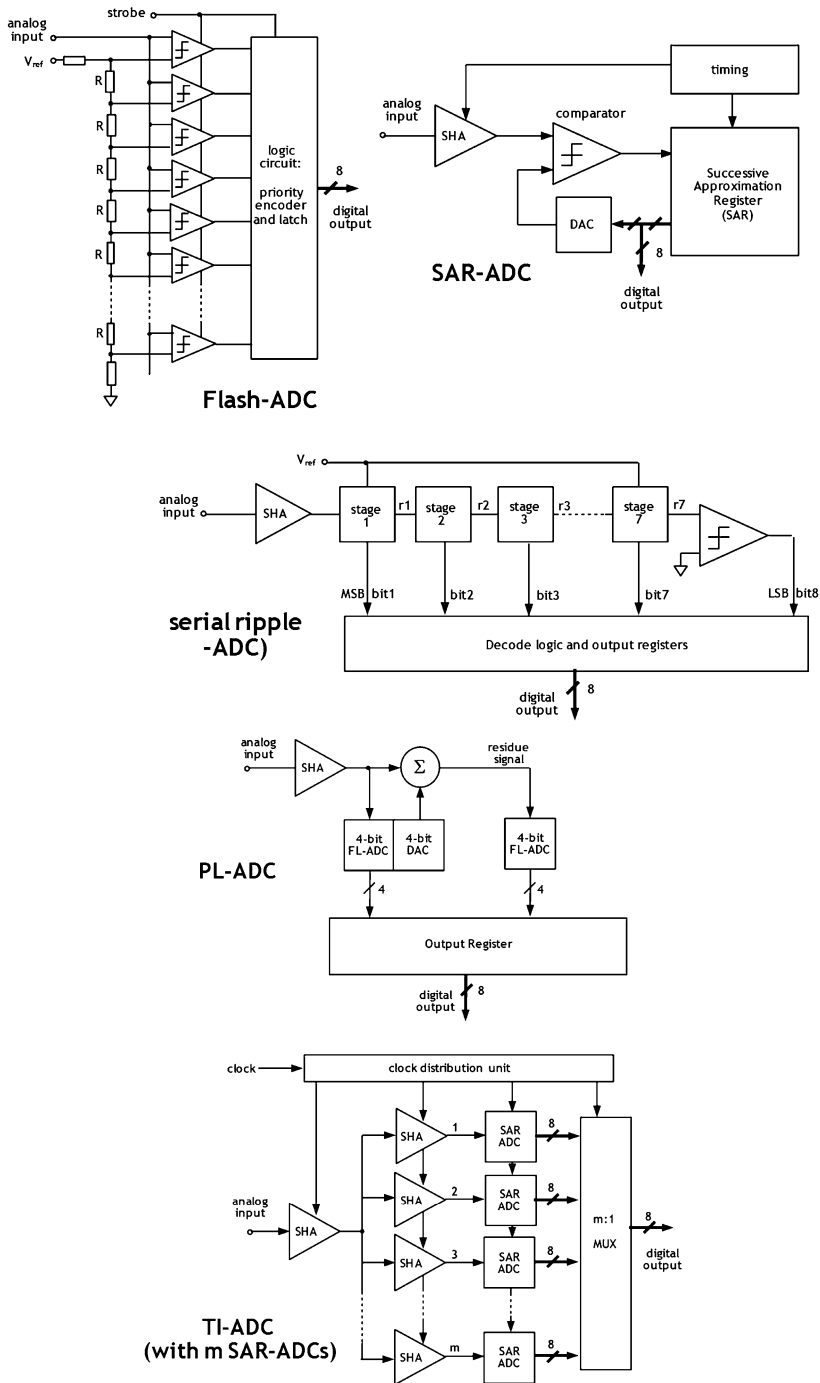


Fig. 7.25 Various ADC architectures (all with 8-bit resolution)

**Table 7.10** Strengths and weaknesses of ADC concepts

Concept	Speed	Latency	Accuracy	Area
FL-ADC	++	++	++	--
SAR-ADC	–	--	+	++
PL-ADC	+	++	+	0
SR-ADC	+	0	0	–
TI-SAR-ADC	++	+	+	0

*Time-interleaved SAR ADC (TI-ADC)*: TI-ADCs use  $m$  parallel sub-ADCs where each sub-ADC samples data every  $m$ th cycle of the effective sampling clock. Thus, each sub-ADC needs to manage an  $m$ -times lower sampling rate only which results in a very high aggregate throughput. The sub-ADCs in the time-interleaved approach are usually SAR ADCs. The challenges of TI-SAR ADCs are the clock distribution and the handling of mismatch and de-skew between the sub-ADCs. The time-interleaving concept enables the use of lower speed CMOS circuits for ADCs with multi-G sampling rates [25]. The input bandwidth of the TI-SAR ADC is determined by the first set of SHAs.

Table 7.10 indicates where the different ADC concepts have particular strengths (++ or +), weaknesses (– or --) or exhibit neutral performance (0).

ADCs and DACs for optical communication have been realized by different technologies and their performance will be discussed in the section on ASIC technologies (Sect. 7.7.3).

## 7.7 Devices for Coherent Transceivers

As mentioned above IQ modulators are particularly suited for square-QAM formats due to the regular structure of the constellation projected onto the in-phase and quadrature axis. Various alternative modulator and transmitter structures with separate amplitude and phase modulator stages to better support the modulation of various ASK-PSK modulation formats and which are suited for direct detection (DD) have been discussed in detail in [127]. In addition, a variety of hybrid optical structures for coherent and DD receivers have also been treated in [127].

The laser phase noise issue, one of the biggest problems of coherent systems in the past, has been overcome by the implementation of better frequency and phase correction algorithms. As laser phase noise scales with the symbol rate, the use of high symbol rates relaxes phase noise issues even further. By continuously increasing sampling rates of DACs and ADCs, the symbol rate of transmission systems has been increased significantly compared to the first coherent transceivers operating at 40 Gbit/s with symbol rates of 10 GBd. The pessimistic picture of laser phase noise given in [127] had been derived from the idea of applying HOM formats at 40 Gbit/s on a single polarization which would have resulted in symbol rates well

below 10 GBd, e.g. 6.4 GBd for 16QAM. Finally, low linewidth lasers for coherent transceivers with 100 kHz linewidth and even 4 kHz lasers [128] have become commercially available.

In the following section we will concentrate on dual-polarization IQ modulators and coherent receiver frontends for coherent detection for a single and for dual sub-carrier FDM solutions. Beyond the OE frontends, the ASIC technology requirements and limitations for the realization of data converters and DSP are addressed and recent ASIC chips realized for optical communications are summarized.

### 7.7.1 Dual Polarization IQ Modulators

We will focus on the ideal modulator for square-QAM operated in a dual polarization mode. This is the dual polarization IQ modulator which has become commercially available in 2009, and the package and performance parameters of this DP-IQ modulator have been specified by the OIF Implementation Agreement (IA) [31] in 2010. Initially the OIF-IA was intended to specifically address 100G DP-QPSK applications including FEC and supporting symbol rates up to 32 GBd.

#### 7.7.1.1 Single and Dual Carrier IQ Modulators

Figure 7.10 of Sect. 7.3.1.5 illustrated the generic structure of a DP-IQ modulator for the modulation of a single carrier wavelength in  $x$  and  $y$  polarization by two separate nested or mother MZM structures. We call this structure version 1 (v1). A potential future integrated 2nd version (v2) of a DP-IQ modulator is shown in Fig. 7.26 (left side), including integrated lasers, either monolithically integrated on InP or hybridly integrated on GaAs or Si. Another important feature is related to the driving path from the DAC to the modulator. The modulator requires voltages which cannot be delivered fully by the converter itself. Therefore driver-less operation or an integrated driver option are important alternatives to save volume and reduce power consumption. Figure 7.26 also includes a future two sub-carrier FDM modulator which has significantly higher complexity.

Each IQ mother MZM consists of two child MZMs, the I- and Q-MZM, and a  $90^\circ$  phase shifter ( $\pi/2$ ). The OIF-IA specifies four single ended GPPO modulation inputs per child MZM while all DC bias segments are usually implemented differentially (n and p) at the bias segments of both child and the mother MZM. This is in contrast to the principle shown in Fig. 7.26 where only one branch of the mother MZM includes the  $90^\circ$  phase shift element. Laser light is injected via a polarization maintaining fiber and split and separately modulated by the mother MZMs. The modulated output of one mother MZM is polarization rotated and combined with the second in a polarization beam combiner resulting in two modulated signals having two polarizations orthogonal to each other.

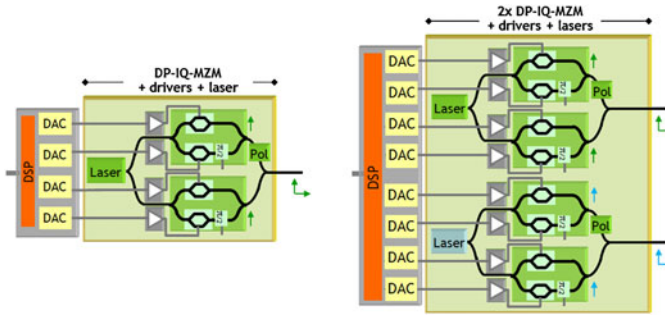


**Fig. 7.26** Single and dual sub-carrier (FDM) dual-polarization IQ modulator structures in future (potentially integrated) version (v2). Pol: polarization rotator,  $\varphi$ :  $90^\circ$  phase shifter

In order to modulate BPSK or MQAM signals, the DC bias voltages of all four child MZMs are set to the minimum transmission point  $V_{bias} = V_\pi$ , and the modulation swing is chosen to be  $V_{mod} = V_{2\pi}$ . Modulators with low  $V_\pi$  are desirable in order to minimize driver voltages and power consumption. A major design issue of MZMs is the trade-off between achieving low  $V_\pi$  and high modulation bandwidth at the same time. The main performance parameters of DP-IQ modulators are: total minimum insertion loss, modulation voltage  $V_\pi$  at 1 GHz, modulation bandwidth, minimum extinction ratio including all child and mother MZMs, and skewing of the four modulation paths  $I_x$ ,  $Q_x$ ,  $I_y$ , and  $Q_y$ . The minimum insertion loss is measured when all modulators are biased at maximum transmission. Extinction ratios are measured between bias at maximum and minimum transmission corresponding to the individual child or mother MZM.

The first commercially available DP-IQ modulator was based upon a  $\text{LiNbO}_3$  z-cut modulator structure and since 2013, InP- and GaAs technology based dual-polarization IQ modulators compliant with the OIF-IA have also become commercially available which have the advantage of enabling significantly smaller form factors. The same holds for Si-based modulators [129] which have already been integrated together with a coherent frontend [130].

In [127] modulation voltages  $V_\pi$  specified for various  $\text{LiNbO}_3$  modulators have been summarized, and they vary between 4 V and 7.5 V so that a four child DP-IQ MZM requires four channel drivers with  $4 \times 8$  V and  $4 \times 15$  V, respectively. None of these drivers is available today. However, due to an attractive  $V_\pi$  value reported in [131] (reduced to  $\sim 3$  V) in combination with attractive volume prices of dual polarization modulators, thousands of  $\text{LiNbO}_3$  DP-IQ modulators have been shipped since 2010 and have been implemented in most 100G transceivers.

The first 400G transceivers which include two sub-carrier FDM DP-16QAM have been implemented using two separate DP-IQ modulators with two separate four channel modulator drivers. Since 2015 a  $\text{LiNbO}_3$  modulator package is commercially available which includes two DP-IQ modulators and also eight integrated channel modulator drivers to be connected with  $8 \times$  G3PO connectors for modula-

tion of the eight child MZMs. Figure 7.26 includes a future two sub-carrier FDM DP-IQ modulator with integrated laser and drivers.

1 Tbit/s two sub-carrier FDM transceivers require symbol rates of 53 GBd or 64 GBd together with DP-64QAM or DP-32QAM modulation, respectively, as shown in Table 7.8.

### 7.7.1.2 Multiple Carrier IQ Modulators

The first integrated multiple sub-carrier IQ modulators have been based upon InP technology with a monolithically integrated PIC [132] implemented in FDM transmitters. The PIC comprises 10 IQ modulators, 10 tuneable DFB lasers and an arrayed waveguide grating (AWG) serving as wavelength combiner. InP PIC chips were also incorporated in coherent FDM transceivers including 10-fold QPSK modulations.

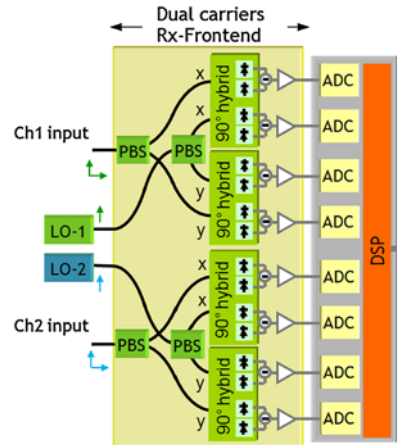
These FDM transmitters did not include DACs and focused on binary modulation only, as a transceiver with 40 DACs and ADCs can hardly be realized due to power consumption issues. Thus, these FDM transmitters with a high number of sub-carriers have no potential for the optimization of the spectral efficiency by higher constellation MQAM formats including shaping.

## 7.7.2 Optical Receiver Frontend

Similar to the modulator case, component providers agreed also on a preferred solution for a polarization diversity coherent receiver frontend. In 2010 the OIF published the implementation agreement for an integrated intradyne coherent receiver also suitable for 100 Gbit/s DP-QPSK systems up to symbol rates of 32 GBd.

The basic structure of the frontend was shown in Fig. 7.10 (Sect. 7.3.1.5). Figure 7.27 includes a potential future integrated two sub-carrier FDM solution on Si with hybridly integrated local oscillator lasers. The chip has two input fibers allowing highest flexibility. For each single carrier path the received signal (coupled in from a standard fiber) is split by a polarization beam splitter, and the  $x$  and  $y$  polarization components of the signal interfere with the light of the LO laser in  $2 \times 2$   $90^\circ$  hybrids. The splitting of the LO light by another PBS is shown schematically but in reality the separated polarization components of the information signal exhibit the same linear polarization state at the PBS outputs, and it is therefore sufficient that the LO light, the polarization of which must be aligned to the polarization of the signal at the two PBS outputs, is equally split by a 3 dB coupler. The output signals of the  $2 \times 2$   $90^\circ$  hybrids are detected by four pairs of balanced photodiodes and amplified by linear TIAs. The outputs of the O/E frontend provide the in-phase and quadrature photocurrents of both polarization components:  $I_x$ ,  $Q_x$ ,  $I_y$ , and  $Q_y$  for both carriers, digitally converted by four ADCs and then further processed by

**Fig. 7.27** Future two sub-carrier FDM frontend



digital signal processing. A two sub-carrier receiver simply doubles the components and complexity.

The key elements of the receivers are SMF input fibers for each sub-carrier which allow highest flexibility at the Rx, PM fiber inputs for external local oscillator lasers, 90° hybrids, balanced photodetectors, linear TIAs, all channels selectable with manual or automatic gain control, and coplanar RF input interfaces.

### 7.7.3 ASIC Technologies

The first DACs and ADCs were implemented in fiber optic communication in 10 Gbit/s intensity modulated and direct detection (IM-DD) systems in 2005. The purpose was the compensation of linear transmission distortions such as chromatic dispersion in the electronic domain. The first ADC chip supported over-sampling with 20 GSamples/s and 3-bit resolution, and was applied at the receiver side together with a digital equalizer (DEQ) chip for electronic dispersion post-compensation. In a multi-chip transceiver the ADC was implemented based upon 200 GHz SiGe bipolar technology while the DEQ chip based on a Viterbi decoder was realized by 130 nm CMOS technology. The first dual DAC supporting sampling with 22 GSamples/s and 5-bit resolution integrated in a single ASIC together with the transmitter DSP with FIR filter taps for electronic pre-compensation, was realized by 130 nm SiGe BiCMOS [133] technology.

Silicon technologies underwent significant progress by doubling the transistor count every two years. Between the introduction of digital converters and DSP in optical communication in 2005 and 2015 the number of gates and functionalities realized and implemented in application-specific integrated circuits has been increased very significantly. It is worthwhile to note that Moore’s law is still alive but applies to the chip density and not anymore to transistor speed, and 16 nm CMOS



technology reaches four times higher density than 28 nm CMOS technology applied in the 2014 generation of optical transceiver ASICs.

High-speed data converters have been realized in CMOS- or in SiGe-based bipolar technology. Due to a high degree of parallelization, CMOS favors high-sampling rate designs while SiGe bipolar supports higher bandwidth. Dual-chip solutions with a SiGe-based data converter and DSP in CMOS technology provide converters with optimum frequency response and allow the use of advanced CMOS technology for the DSP part. Unfortunately, this dual-chip approach leads to significant challenges with respect to high volume data transfer between the data converter ASIC and the DSP ASIC, and with respect to the resolution and sampling rate requirements of current and future 400G implementations, it becomes mandatory to co-integrate converters with the DSP. For example, in the 28 nm CMOS ASIC generation for optical transceivers, four DACs, each performing at least theoretically with 8-bit resolution and 92 GSamples/s maximum sampling rate, require a total transfer rate between DAC and DSP of  $4 \times 8 \times 92 = 2.944$  Tbit/s. This can only be handled in a single CMOS ASIC chip solution.

In the first coherent transceiver generation the FEC was not fully integrated with DSP ASIC chips while in 2015 commercial coherent transceiver products comprise fully customized CMOS ASICs which offer best performance and lowest power consumption, however, at the expense of complexity and costly design cycles. DSP and FEC require purely digital functions and can be realized best in CMOS technology. Data converters include analogue and digital functions and are therefore also called ‘mixed signal’ circuits. Because of the stringent requirements concerning sampling speed, bandwidth, and signal integrity, they require a different design methodology than DSP and FEC. Typically, a full custom design procedure is implemented for the design of data converters and sampling speeds considered for symbol rates beyond 32 GBd. For analogue parts and even critical digital parts, the circuit layout is done manually and parasitic extraction is performed to augment the circuit simulation with more realistic models. In latest generation 28 nm CMOS technology, SD-FEC as well as Tx DSP and Rx DSP, eight DACs and eight ADCs required for a 400 Gbit/s transceiver with two sub-carriers can be implemented in a single ASIC chip. Single ASICs for 1 Tbit/s transceivers with up to five sub-carriers and twenty DACs and twenty ADCs are not expected to pose major problems arising from the number of supported carriers per ASIC chip if the ASIC is fabricated using the newest 16 nm CMOS technology, however, how to get the signals out of the ASIC package will probably be a demanding task.

Tables 7.11 and 7.12 summarize technologies which are used in optical communication and the focus is on data converters and integration (yes or no) with DSP functions. The tables indicate converter concepts, their maximum sampling rate and theoretical resolution, the die size, and power consumption. For most recent CMOS based DACs and ADCs the integration of DSP became mandatory and the applied concepts are usually segmented DACs and time-interleaved SAR ADCs. The tables also show the progress in sampling speed and power consumption obtained by CMOS technologies. Attractive high sampling speed has been achieved with

**Table 7.11** Evolution and key parameters of DACs applied in optical transceiver ASICs or instrumentation

Source	Technology	Year	Tx-DSP integr.?	DAC Concept	Resolution (bits)	Max. Sampling Rate (GSamples/s)	Die size (mm <sup>2</sup> )	Power (W)	Ref.
Nortel	13C-nm SiGe BiCMOS	2005	Yes	SEG (TM&R-2R)	6	22	2.5 × 1.8	1.2	[134]
NTT	1-µm InP HBT	2009	No	R-2R	6	32	3 × 3	1.4	[135]
IHP	250-nm SiGe BiCMOS	2008	No	SEG (TM&R-2R)	8	20	2 × 3	2.5	[136]
Micram	SiGe BiCMOS	2010	No	BW	6	34	5 × 5	0.4	[137]
Nortel	65-nm CMOS	2011	Yes	SEG (TM&BW)	6	56	0.6 × 0.4	0.75	[138]
NTT	0.5-µm InP HBT	2011	No	R-2R	6	60	3 × 3	1.8	[139]
Fujitsu	40-nm CMOS	2012	Yes	SEG	8	65	-	0.75	[140]
Tek	SiGe BiCMOS	2013	-	-	10	25	-	-	[141]
Fujitsu	28-nm CMOS	2014	Yes	SEG	8	92	-	-	[75]

**Table 7.12** Evolution and key parameters of ADCs applied in optical transceiver ASICs or instrumentation

Source/Foundry	Technology	Year	Rx-DSP integr.?	ADC Concept	Resolution (bits)	Max. Sampling Rate (GSamples/s)	Die Size (mm <sup>2</sup> )	Power (W)	Ref.
Agilent	180-nm CMOS	2003	No	PL	8	35	14 × 14	9	[142]
Nortel/STM	130-nm SiGe BiCMOS	2006	No	FL	5	22	1.8 × 2.5	3	[143]
Alcatel-Lucent	180-nm SiGe BiCMOS	2008	No	FL	5	24	2.6 × 3.3	3.3	[144]
Nortel	90-nm CMOS	2008	Yes	TI-SAR	6	24	4 × 4	1.2	[145]
Micram	SiGe HBT/BiCMOS	2010	Yes	SR	6	34	1 × 2.6	2	[137]
Ciena	65-nm CMOS	2010	Yes	TI-SAR	6	40	4 × 4	1.5	[138]
Fujitsu	65-nm CMOS	2010	Yes	TI-SAR	8	56	-	2	[146]
Fujitsu	40-nm CMOS	2012	Yes	TI-SAR	8	65	-	1.2	[147]
Fujitsu	28-nm CMOS	2013	Yes	TI-SAR	8	92	-	<1	[148]

CMOS and the power consumption has been continuously decreased with technology progress. Even higher sampling rates than 100 GSamples/s are probably feasible with CMOS but the current trend of ASIC design is to further reduce the power consumption instead of increasing the sampling speed.

## References

1. [www.cisco.com/c/en/us/solutions/collateral/service-provider/ip-ngn-ip-next-generation-network/white\\_paper\\_c11-481360.html](http://www.cisco.com/c/en/us/solutions/collateral/service-provider/ip-ngn-ip-next-generation-network/white_paper_c11-481360.html)
2. R.W. Tkach, Scaling optical communications for the next decade and beyond. *Bell Labs Tech. J.* **14**(4), 3–10 (2010)
3. B. Wedding, W. Idler, B. Franz, W. Pöhlmann, E. Lach, 40 Gbit/s quaternary dispersion supported transmission over 31 km of standard single mode fibre without optical dispersion compensation, in *Proc. 24th Europ. Conf. Opt. Commun.* (ECOC'98), Madrid, Spain (1998), paper WdCO8
4. C. Xie, S. Spiga, P. Dong, P. Winzer, M. Bergmann, B. Koegel, C. Neumeyr, M. Amann, 400-Gb/s PDM-4PAM WDM system using a monolithic  $2 \times 4$  VCSEL array and coherent detection. *J. Lightwave Technol.* **33**(3), 670–677 (2015)
5. J.M. Kahn, K. Ho, Spectral efficiency limits and modulation/detection techniques for DWDM systems. *IEEE J. Sel. Top. Quantum Electron.* **10**, 259–279 (2004)
6. Y. Koizumi, K. Toyoda, M. Yoshida, M. Nakazawa, 1024 QAM (60 Gbit/s) single-carrier coherent optical transmission over 150 km. *Opt. Express* **20**(11), 12508–12514 (2012)
7. S. Beppu, K. Kasai, M. Yoshida, N. Nakazawa, 2048 QAM (66 Gbit/s) single-carrier coherent optical transmission over 150 km with a potential SE of 15.3 bit/s/Hz. *Opt. Express* **23**(4), 4960–4969 (2015)
8. Optical internetworking document: 100G ultra long haul DWDM framework document. OIF-FD-100G-DWDM-01.0.pdf
9. Dell'Oro Group, Optical transport market report 2Q16, Market summary and vendor information **18**(2), O1A
10. <http://www.lightwaveonline.com/articles/2016/01/100g-200g-wdm-to-drive-optical-transport-sales-growth-through-2020-delloro.html>
11. S.L. Jansen, I. Morita, K. Forozesh, S. Randel, D. van den Borne, H. Tanaka, Optical OFDM, a hype or is it for real? in *Proc. 24th Europ. Conf. Opt. Commun.* (ECOC'98), Madrid, Spain (1998), paper Mo.3.E.3
12. A. Bononi, N. Rossi, P. Serena, Transmission limitations due to fibre nonlinearity, in *Opt. Fiber Commun. Conf. and Nat. Fiber Opt. Eng. Conf.* (OFC/NFOEC'11), Los Angeles, CA, USA (2011), Techn. Digest, paper OWO7
13. W. Yan, T. Tanaka, B. Liu, M. Nishihara, L. Li, T. Takahara, Z. Tao, J.C. Rasmussen, T. Drenski, 100 Gb/s optical IM-DD transmission with 10G-class devices enabled by 65 GSamples/s CMOS DAC core, in *Opt. Fiber Commun. Conf. and Nat. Fiber Opt. Eng. Conf.* (OFC/NFOEC'13), Anaheim, CA, USA (2013), Techn. Digest, paper OM3H1
14. T. Tanaka, M. Nishihara, T. Takahara, W. Yan, L. Li, Z. Tao, M. Matsuda, K. Takabayashi, J.C. Rasmussen, Experimental demonstration of 448-Gbps DMT transmission over 30-km SMF, in *Opt. Fiber Commun. Conf.* (OFC'14), San Francisco, CA, USA (2014), Techn. Digest, paper M2I5
15. ITU-T recommendation G.694.2, Spectral grids for WDM applications: CWDM wavelength grid, published 12/2003
16. A. Sano, H. Masuda, T. Kobayashi, M. Fujiwara, K. Horikoshi, E. Yoshida, Y. Miyamoto, M. Matsui, M. Mizoguchi, H. Yamazaki, Y. Sakamaki, H. Ishii, 69.1-Tb/s ( $432 \times 171$ -Gb/s) C- and extended L-band transmission over 240 km using PDM-16-QAM modulation and

- digital coherent detection, in *Opt. Fiber Commun. Conf. and Nat. Fiber Opt. Eng. Conf.*, (OFC/NFOEC'10), San Diego, CA, USA (2010), Techn. Digest, paper PDPB7
17. S. Makovejs, C.C. Roberts, F. Palacios, H.B. Matthews, D.A. Lewis, D.T. Smith, P.G. Diehl, J.J. Johnson, J.D. Patterson, C.R. Towery, S.Y. Ten, Record-low (0.1460 dB/km) attenuation ultra-large  $A_{eff}$  optical fiber for submarine applications, in *Opt. Fiber Commun. Conf.* (OFC'15), Los Angeles, CA, USA (2015), Techn. Digest, PDP Th5A2
  18. S. Randel, Space-division multiplexed transmission, in *Opt. Fiber Commun. Conf. and Nat. Fiber Opt. Eng. Conf.* (OFC/NFOEC'13), Anaheim, CA, USA (2013), Techn. Digest, paper OW4F1
  19. K. Igarashi, D. Souma, Y. Wakayama, K. Takeshima, Y. Kawaguchi, T. Tsuritani, I. Morita, M. Suzuki, 114 space-division-multiplexed transmission over 9.8-km weakly-coupled-6-mode uncoupled-19-core fibers, in *Opt. Fiber Commun. Conf.* (OFC'15), Los Angeles, CA, USA (2015), Techn. Digest, PDP Th5C.4
  20. N.K. Fontaine, R. Ryf, H. Chen, A. Velazquez Benitez, J.E. Antonio-Lopez, R. Amezcua-Correa, B. Guan, B. Ercan, R.P. Scott, S.B. Yoo, L. Grueuner-Nielsen, Y. Sun, R. Lingle,  $30 \times 30$  MIMO transmission over 15 spatial modes, in *Opt. Fiber Commun. Conf.* (OFC'15), Los Angeles, CA, USA (2015), Techn. Digest, PDP Th5C.1
  21. T.J. Xia, G. Wellbrock, B. Basch, S. Kotrla, W. Lee, T. Tajima, K. Fukuchi, M. Cvijetic, J. Sugg, Y. Ma, B. Turner, C. Coole, C. Urricariet, End-to-end native IP data 100G single carrier real time DSP coherent detection transport over 1520-km field deployed fiber, in *Opt. Fiber Commun. Conf. and Nat. Fiber Opt. Eng. Conf.* (OFC/NFOEC'10), San Diego, CA, USA (2010), Techn. Digest, paper PDP D4
  22. P.W. Hooijmans, *Coherent Optical System Design* (Wiley, Chichester, 1994)
  23. L.G. Kazovsky, R. Welter, A.F. Elrefaie, W. Sessa, Wide-linewidth phase diversity homodyne receivers. *J. Lightwave Technol.* **6**, 1527–1536 (1988)
  24. S. Norimatsu, K. Iwashita, K. Noguchi, An 8 Gb/s QPSK optical homodyne detection experiment using external-cavity laser diodes. *IEEE Photonics Technol. Lett.* **4**, 765–767 (1992)
  25. L.G. Kazovsky, G. Kalogerakis, W.T. Shaw, Homodyne phase-shift-keying systems: past, challenges and future opportunities. *J. Lightwave Technol.* **24**, 4876–4884 (2006)
  26. J.H. Winters, Equalization in coherent lightwave systems using a fractionally spaced equalizer. *J. Lightwave Technol.* **8**, 1487–1491 (1990)
  27. B. Spinnler, P.M. Krummrich, E.-D. Schmidt, Chromatic dispersion tolerance of coherent optical communication systems with electrical equalization, in *Opt. Fiber Commun. Conf.* (OFC'06), Anaheim, CA, USA (2006), Techn. Digest, paper OWB2
  28. T. Pfau, S. Hoffmann, R. Peveling, S. Bhandare, S.K. Ibrahim, O. Adamczyk, M. Pormann, R. Noé, Y. Achiam, First real-time data recovery for synchronous QPSK transmission with standard DFB lasers. *IEEE Photonics Technol. Lett.* **18**, 1907–1909 (2006)
  29. [www.lightwaveonline.com](http://www.lightwaveonline.com), *Lightwave*, **27**(1) and **27**(2) (2010)
  30. E. Lach, W. Idler, Modulation formats for 100G and beyond. *Opt. Fiber Technol.* **17**(5), 377–386 (2011)
  31. Optical Internetworking Forum (OIF): Implementation agreement for integrated polarization multiplexed quadrature modulated transmitters, doc. IA # OIF-PMQ-TX-01.0, March, 2010
  32. Optical Internetworking Forum (OIF): Implementation agreement for integrated dual polarization intradyne coherent receivers, doc. IA#OIF-DPC-RX-01.1, Sept. 2011
  33. IEEE Standard 802.3ba-2010, Amendment 4: Media access control parameters, physical layers and management parameters for 40 Gb/s and 100 Gb/s operation, June 2010
  34. ITU-T recommendation G.709: Interfaces for the optical transport network (OTN), published Dec. 2009
  35. J. D'Ambrosia, 100 Gigabit Ethernet and beyond. *IEEE Commun. Mag.* **48**(3), S6–S13 (2010)
  36. Optical Internetworking Forum (OIF) document, 100G forward error correction, White Paper, May 2010, OIF-FEC-100G-01.0
  37. F. Gray, Pulse code communication, US Patent 2632058, 1953

38. C.E. Shannon, A mathematical theory of communication. *Bell Syst. Tech. J.* **27**, 379–423 and 623–656 (1948)
39. R. Hartley, Transmission of information, in *Intern. Congress on Telegraphy and Telephony*, Como, Italy (1927)
40. C.N. Campopiano, B.G. Glazer, A coherent digital amplitude and phase modulation system. *IRE Trans. Commun. Syst.* **CS-10**, 90–95 (1962)
41. G. Ungerboeck, Channel coding with multilevel/phase signals. *IEEE Trans. Inf. Theory* **28**(1), 55–67 (1982)
42. J.G. Proakis, *Digital Communications*, 4th edn. (McGraw–Hill, Singapore, 2001)
43. R.J. Essiambre, G. Kramer, P. Winzer, G. Foschini, B. Goebel, Capacity limits of optical fiber networks. *J. Lightwave Technol.* **28**(4), 662–701 (2010)
44. A. Alvarado, E. Agrell, D. Lavery, P. Bayvel, LDPC codes for optical channels: is the FEC limit a good predictor of post-FEC BER? in *Opt. Fiber Commun. Conf. (OFC'15)*, Los Angeles, CA, USA (2015), Techn. Digest, paper Th3E.5
45. W.R. Peng, I. Morita, H. Tanaka, Hybrid QAM transmission techniques for single-carrier ultra-dense WDM systems, in *Optoelectron. Commun. Conf. (OECC 2011)*, Taiwan, (2011), Techn. Digest, paper 8D2-4
46. Q. Zhuge, X. Xu, M. Morsy-Osman, M. Chagnon, M. Qiu, D.V. Plant, Time domain hybrid QAM based rate-adaptive optical transmissions using high speed DACs, in *Opt. Fiber Commun. Conf. and Nat. Fiber Opt. Eng. Conf. (OFC/NFOEC'13)*, Anaheim, CA, USA (2013), Techn. Digest, paper OTh4E6
47. F. Buchali, L. Schmalen, K. Schuh, W. Idler, Optimization of time-division hybrid-modulation and its application to rate adaptive 200 Gb transmission, in *Proc. 40th Europ. Conf. Opt. Commun. (ECOC'14)*, Cannes, France (2014), paper Tu.4.3.1
48. W. Idler, F. Buchali, L. Schmalen, K. Schuh, H. Buelow, Hybrid modulation formats outperforming 16QAM and 8QAM in transmission distance and filtering with cascaded WSS, in *Opt. Fiber Commun. Conf. (OFC'15)*, Los Angeles, CA, USA (2015), Techn. Digest, paper M3G4
49. P.J. Winzer, A.H. Gnauck, 112-Gb/s polarization-multiplexed 16-QAM on a 25-GHz WDM grid, in *Proc. 34th Europ. Conf. Opt. Commun. (ECOC'08)*, Brussels, Belgium (2008), PDP Th3.E.5
50. M. Nölle, J. Hilt, M. Seimetz, R. Freund,  $8 \times 224$  Gb/s PDM 16QAM WDM transmission with real-time signal processing at the transmitter, in *Proc. 36th Europ. Conf. Opt. Commun. (ECOC'10)*, Torino, Italy (2010), paper We.8.C.4
51. A.H. Gnauck, P.J. Winzer, A. Konczykowska, F. Jorge, J. Dupuy, M. Riet, G. Charlet, B. Zhu, D.W. Peckham, Generation and transmission of 21.4 Gbaud PDM 64 QAM using a high power DAC driving a single I/Q modulator, in *Opt. Fiber Commun. Conf. and Nat. Fiber Opt. Eng. Conf. (OFC/NFOEC'11)*, Los Angeles, CA, USA (2011), Techn. Digest, paper PDPB2
52. H. Buelow, X. Lu, L. Schmalen, A. Klekamp, F. Buchali, Experimental performance of 4D optimized constellation – alternatives for PM-8QAM and PM-16QAM, in *Opt. Fiber Commun. Conf. and Nat. Fiber Opt. Eng. Conf. (OFC/NFOEC'14)*, San Francisco, CA, USA (2014), Techn. Digest, paper M2A.6
53. X. Zhou, J. Yu, M.-F. Huang, Y. Shao, T. Wang, L. Nelson, P. Magill, M. Birk, P.I. Borel, D.W. Peckham, R. Lingle, 64-Tb/s ( $640 \times 107$ -Gb/s) PDM-36QAM transmission over 320 km using both pre- and post-transmission digital equalization, in *Opt. Fiber Commun. Conf. and Nat. Fiber Opt. Eng. Conf. (OFC/NFOEC'10)*, San Diego, CA, USA (2010), Techn. Digest, paper PDPB9
54. A. Sano, T. Kobayashi, A. Matsuura, S. Yamamoto, S. Yamanaka, E. Yoshida, Y. Miyamoto, M. Matsui, M. Mizoguchi, T. Mizuno,  $100 \times 120$ -Gb/s PDM 64-QAM transmission over 160 km using linewidth-tolerant pilotless digital coherent detection, in *Proc. 36th Europ. Conf. Opt. Commun. (ECOC'10)*, Torino, Italy (2010), paper PD2.4
55. A. Sano, T. Kobayashi, K. Ishihara, H. Masuda, S. Yamamoto, K. Mori, E. Yamazaki, E. Yoshida, Y. Miyamoto, T. Yamada, H. Yamazaki, 240-Gb/s polarization-multiplexed 64-

- QAM modulation and blind detection using PLC-LN hybrid integrated modulator and digital coherent receiver, in *Proc. 35th Europ. Conf. Opt. Commun.* (ECOC'09), Vienna, Austria (2009), paper PD2.2
56. T. Kobayashi, A. Sano, A. Matsuura, Y. Miyamoto, K. Ishihara, High-order QAM transmission for spectrally-efficient and high-capacity transport, in *Opt. Fiber Commun. Conf. and Nat. Fiber Opt. Eng. Conf.* (OFC/NFOEC'12), Los Angeles, CA, USA (2012), Techn. Digest, paper OM2A3
  57. M. Nakazawa, S. Okamoto, T. Omiya, K. Kasai, M. Yoshida, 256 QAM (64 Gbit/s) coherent optical transmission over 160 km with an optical bandwidth of 5.4 GHz, in *Opt. Fiber Commun. Conf. and Nat. Fiber Opt. Eng. Conf.* (OFC/NFOEC'10), San Diego, CA, USA (2010), Techn. Digest, paper OMJ5
  58. S. Okamoto, K. Toyoda, T. Omiya, K. Kasai, M. Yoshida, M. Nakazawa, 512 QAM (54 Gb/s) coherent optical transmission over 150 km with an optical bandwidth of 4.1 GHz, in *Proc. 36th Europ. Conf. Opt. Commun.* (ECOC'10), Torino, Italy (2010), paper PD2.3
  59. D. Qian, M.-F. Huang, E. Ip, Y.-K. Huang, Y. Shao, J. Hu, T. Wang, 101.7-Tb/s ( $370 \times 294$ -Gb/s) PDM-128QAM-OFDM Transmission over  $3 \times 55$ -km SSMF using pilot-based phase noise mitigation, in *Opt. Fiber Commun. Conf. and Nat. Fiber Opt. Eng. Conf.* (OFC/NFOEC'11), Los Angeles, CA, USA (2011), Techn. Digest, paper PDPB5
  60. X. Liu, S. Chandrashekar, Superchannel for next-generation optical networks, in *Opt. Fiber Commun. Conf.* (OFC'14), San Francisco, CA, USA (2014), Techn. Digest, tutorial WH1.5
  61. ITU-T recommendation G.694.1: Spectral grids for WDM applications: DWDM frequency grid, published 2012
  62. G. Raybon, A.L. Adamiecki, P. Winzer, C. Xie, A. Konczykowska, F. Jorge, J.-Y. Dupuy, L.L. Buhl, S. Chandrashekar, S. Draving, M. Grove, K. Rush, Single-carrier 400G interface and 10-channel WDM transmission over 4,800 km using all-ETDM 107-Gbaud PDM-QPSK, in *Opt. Fiber Commun. Conf. and Nat. Fiber Opt. Eng. Conf.* (OFC/NFOEC'13), Anaheim, CA, USA (2013), Techn. Digest, paper PDP5A.5
  63. R. Rios-Müller, J. Renaudier, P. Brindel, H. Mardoyan, P. Jennevé, L. Schmalen, G. Charlet, 1-Terabit/s net data-rate transceiver based on single-carrier Nyquist-shaped 124 GBaud PDM-32QAM, in *Opt. Fiber Commun. Conf.* (OFC'15), Los Angeles, CA, USA (2015), Techn. Digest, PDP Th5B.1
  64. G. Raybon, A. Adamiecki, P. Winzer, S. Randel, L. Salamanca, A. Konczykowska, F. Jorge, J. Dupuy, L. Buhl, S. Chandrashekar, C. Xie, S. Draving, M. Grove, K. Rush, R. Urbanke, High symbol rate coherent optical transmission systems: 80 and 107 Gbaud. *J. Lightwave Technol.* **32**(4), 824–831 (2014)
  65. G. Raybon, A. Adamiecki, P.J. Winzer, M. Montoliu, S. Randel, A. Umbach, M. Margraf, J. Stephan, S. Draving, M. Grove, K. Rush, All-ETDM 107-Gbaud PDM-16QAM (856-Gb/s) transmitter and coherent receiver, in *Proc. 39th Europ. Conf. Opt. Commun.* (ECOC'13), London, UK (2013), paper PD2D3
  66. O. Bertran-Pardo, J. Renaudier, H. Mardoyan, P. Tran, R. Rios-Muller, A. Konczykowska, J.-Y. Dupuy, F. Jorge, M. Riet, B. Duval, J. Godin, S. Randel, G. Charlet, S. Bigo, Transmission of 50-GHz-spaced single-carrier channels at 516 Gb/s over 600 km, in *Opt. Fiber Commun. Conf. and Nat. Fiber Opt. Eng. Conf.* (OFC/NFOEC'13), Anaheim, CA, USA (2013), Techn. Digest, paper OTH4E2
  67. J. Renaudier, R. Rios-Muller, L. Schmalen, M. Salsi, P. Tran, G. Charlet, S. Bigo, 1-Tb/s transceiver spanning over just three 50-GHz frequency slots for long-haul systems, in *Proc. 39th Europ. Conf. Opt. Commun.* (ECOC'13), London, UK (2013), paper PD2D5
  68. S. Randel, O. Bertran-Pardo, H. Mardoyan, P. Tran, G. Charlet, S. Bigo, A. Konczykowska, J.-Y. Dupuy, F. Jorge, M. Riet, J. Godin, Spectral efficiency long-haul transmission of 22 Tb/s using 40-Gbaud PDM-16QAM with coherent detection, in *Opt. Fiber Commun. Conf.* (OFC'14), San Francisco, CA, USA (2014), Techn. Digest, paper OW4C.2
  69. J. Renaudier, R. Rios-Muller, L. Schmalen, M. Salsi, P. Tran, G. Charlet, S. Bigo, Spectrally efficient 1-Tb/s transceivers for long-haul optical systems. *J. Lightwave Technol.* **33**(7), 1452–1458 (2015)

70. F. Buchali, K. Schuh, L. Schmalen, W. Idler, E. Lach, A. Leven, 1-Tbit/s dual-carrier DP-64QAM transmission at 64 GBaud with 40% overhead soft-FEC over 320 km SMF, in *Opt. Fiber Commun. Conf. and Nat. Fiber Opt. Eng. Conf.* (OFC/NFOEC'13), Anaheim, CA, USA (2013), Techn. Digest, paper Th4E.3
71. G. Raybon, S. Randel, A. Adamiecki, P. Winzer, L. Salamance, R. Urbanke, S. Chandrasekhar, A. Konczykowska, F. Jorge, J. Dupuy, L. Buhl, M. Grove, K. Rush, 1-Tb/s dual-carrier 80-Gbaud PDM-16QAM WDM transmission at 5.2 b/s/Hz over 3200 km, in *Proc. Photon. Conf.* (IPC'12) (2012). doi:[10.1109/IPCCon.2012.6359319](https://doi.org/10.1109/IPCCon.2012.6359319)
72. W. Idler, F. Buchali, K. Schuh, N. Cameron, T. Brast, S. Schmid, A. Steffan, 1 Tb/s – 4 × 343 Gb/s subcarriers on 50 GHz grid – transmission over 480 km SMF with 22 GHz bandwidth semiconductor modulator, in *Opt. Fiber Commun. Conf.* (OFC'14), San Francisco, CA, USA (2014), Techn. Digest, paper Th4F.2
73. R. Dischler, L. Schmalen, Transmission of a 1.1 Tb/s super channel in 100 GHz optical bandwidth based on PM-256 QAM and spatially coupled FEC, in *Proc. 40th Europ. Conf. Opt. Commun.* (ECOC'14), Cannes, France (2014), paper We. 1.C.1
74. G. Raybon, A. Adamiecki, S. Randel, P.J. Winzer, Single-carrier and dual-carrier 400-Gb/s and 1.0-Tb/s transmission systems, in *Opt. Fiber Commun. Conf.* (OFC'14), San Francisco, CA, USA (2014), Techn. Digest, paper Th4F1
75. Fujitsu, OOLA 55-92 GSa/s 8-bit DAC family; online: [www.fujitsu.com/cn/en/products/devices/semiconductor/fsp/asic/asic/ipmacro/networkingips/](http://www.fujitsu.com/cn/en/products/devices/semiconductor/fsp/asic/asic/ipmacro/networkingips/)
76. A. Carena, G. Bosco, V. Curri, P. Poggiolini, M. Tapia Taiba, F. Forghieri, Statistical characterization of PM-QPSK signals after propagation in uncompensated fiber links, in *Proc. 36th Europ. Conf. Opt. Commun.* (ECOC'10), Torino, Italy (2010), paper P4.07
77. P. Poggiolini, G. Bosco, A. Carena, V. Curri, Y. Jiang, F. Forghieri, The GN-model of fiber non-linear propagation and its applications. *J. Lightwave Technol.* **32**(4), 694–721 (2014)
78. A. Carena, G. Bosco, V. Curri, Y. Jiang, P. Poggiolini, F. Forghieri, EGN model of non-linear fiber propagation. *Opt. Express* **22**(13), 16335–16362 (2104)
79. ITU-T supplement 39 of G-Series: Optical system design and engineering considerations; published Sept. 2012
80. F. Buchali, G. Böcherer, W. Idler, L. Schmalen, P. Schulte, F. Steiner, Experimental demonstration of capacity increase and rate adaptation by probabilistically shaped 64-QAM, in *Proc. 41st Europ. Conf. Opt. Commun.* (ECOC'15), Cannes, France (2015), paper PDP 3.4
81. P.J. Winzer, A.H. Gnauck, A. Konczykowska, F. Jorge, J.-Y. Dupuy, Penalties from in-band crosstalk for advanced optical modulation formats, in *Proc. 37th Europ. Conf. Opt. Commun.* (ECOC'11), Geneva, Switzerland (2011), paper Tu. 5.B.7
82. F. Buchali, W. Idler, L. Schmalen, K. Schuh, H. Buelow, Performance and advantages of 100 Gb/s QPSK/8QAM hybrid modulation formats, in *Opt. Fiber Commun. Conf.* (OFC'15), Los Angeles, CA, USA (2015), Techn. Digest, paper Th2A.16
83. F. Buchali, F. Steiner, G. Boecherer, L. Schmalen, P. Schulte, W. Idler, Rate adaptation and reach increase by probabilistically shaped 64-QAM: an experimental demonstration. *J. Lightwave Technol.* **34**(7), 1599–1609 (2016)
84. ITU-T recommendation G.975.1, Forward error correction for high bit-rate DWDM submarine systems, published Feb. 2004
85. ITU-T recommendation G.709, Interfaces for the Optical Transport Network (OTN), published Dec. 2009
86. G.D. Forney, *Concatenated Codes* (MIT Press, Cambridge, 1966)
87. T.K. Moon, *Error Correction Coding: Mathematical Methods and Algorithms* (Wiley, New York, 2005)
88. I.B. Djordjevic, M. Arabaci, L.L. Minkov, Next generation FEC for high capacity communication in optical transport network. *J. Lightwave Technol.* **27**(16), 3518–3530 (2009)
89. Y. Miyata, K. Sugihara, W. Matsumoto, K. Onohara, T. Sugihara, K. Kubo, H. Yoshida, T. Mizuochi, A triple-concatenated FEC using soft-decision decoding for 100 Gb/s optical transmission, in *Opt. Fiber Commun. Conf. and Nat. Fiber Opt. Eng. Conf.* (OFC/NFOEC'10), San Diego, CA, USA (2010), Techn. Digest, paper OThL3

90. Optical Internetworking Forum (OIF) document, 100G forward error correction. White Paper, May 2010. OIF-FEC-100G-01.0
91. R. Pyndiah, Near optimum decoding of product codes: block turbo codes. *IEEE Trans. Commun.* **46**(8), 1003–1010 (1998)
92. R.G. Gallager, *Low-Density Parity-Check Codes* (MIT Press, Cambridge, 1963). [www.ldpc-codes.com/papers/Robert\\_Gallager\\_LDPC\\_1963.pdf](http://www.ldpc-codes.com/papers/Robert_Gallager_LDPC_1963.pdf)
93. A. Leven, L. Schmalen, Status and recent advances on forward error correction technologies for lightwave systems. *J. Lightwave Technol.* **32**(16), 2735–2750 (2014)
94. Y. Miyata, K. Kubo, H. Yoshida, T. Mizuoch, Proposal for frame structure of optical channel transport unit employing LDPC codes for 100 Gb/s FEC, in *Opt. Fiber Commun. Conf. and Nat. Fiber Opt. Eng. Conf.* (OFC/NFOEC'09), San Diego, CA, USA (2009), Techn. Digest, paper NThB2
95. L. Schmalen, D. Suikat, D. Rösener, A. Leven, Evaluation of left-terminated spatially coupled LDPC codes for optical communications, in *Proc. 40th Europ. Conf. Opt. Commun.* (ECOC'14), Cannes, France (2014), paper Th.2.3.4
96. L. Schmalen, V. Aref, J. Cho, D. Suikat, D. Roesener, A. Leven, Spatially coupled soft-decision error correction for future lightwave systems. *J. Lightwave Technol.* **33**(5), 1109–1116 (2015)
97. A. Ghazisaeidi, L. Schmalen, I.F. de Jauregui Ruiz, P. Tran, C. Simonneau, P. Brindel, G. Charlet, Transoceanic transmission systems using adaptive multi-rate FECs. *J. Lightwave Technol.* **33**(7), 1479–1487 (2015)
98. J.X. Cai, Y. Sun, H.G. Batshon, M. Mazurczyk, H. Zhang, D.G. Foursa, A.N. Pilipetski, 54 Tb/s transmission over 9,150 km with optimized hybrid Raman-EDFA amplification and coded modulation, in *Proc. 40th Europ. Conf. Opt. Commun.* (ECOC'14), Cannes, France (2014), paper PD.3.3
99. W.R. Bennett, Spectra of quantized signals. *Bell Syst. Tech. J.* **27**, 446–472 (1948). <https://archive.org/details/bstj27-3-446>
100. F. Buchali, A. Klekamp, L. Schmalen, T. Drenski, Implementation of 64QAM at 42.66 GBaud using 1.5 samples per symbol DAC and demonstration of up to 300 km fiber transmission, in *Opt. Fiber Commun. Conf.* (OFC'14), San Francisco, CA, USA (2014), Techn. Digest, paper M2A.1
101. W. Idler, F. Buchali, D. Roesener, E. Lach, A. Leven, Spectral pre-distortion with FPGA and DAC at 448-Gb/s DP-16QAM improving nonlinear threshold power (NLT), in *Opt. Fiber Commun. Conf. and Nat. Fiber Opt. Eng. Conf.* (OFC/NFOEC'13), Anaheim, CA, USA (2013), Techn. Digest, paper Oth3C.1
102. F.M. Gardner, A BPSK/QPSK timing-error detector for sampled receivers. *IEEE Trans. Commun.* **COM-34**, 423–429 (1986)
103. M. Oerder, H. Meyr, Digital filter and square timing recovery. *IEEE Trans. Commun.* **COM-36**, 605–612 (1988)
104. I. Fatadin, S. Savory, D. Ives, Compensation of quadrature imbalance in an optical QPSK coherent receiver. *IEEE Photonics Technol. Lett.* **20**(20), 1733–1735 (2008)
105. A. Leven, L. Schmalen, Implementation aspects of coherent transmit and receive functions in application-specific integrated circuits, in *Optical Fibre Telecommunications VIA, Systems and Networks*, 6th edn., vol. 15 (Elsevier, Amsterdam, 2013), pp. 555–585
106. M. Kuschnerov, F.N. Hauske, K. Piyawanno, B. Spinnler, E.-D. Schmidt, B. Lankl, Joint equalization and timing recovery for coherent fiber optic receivers, in *Proc. 34th Europ. Conf. Opt. Commun.* (ECOC'08), Brussels, Belgium (2008), paper Mo3D3
107. S.J. Savory, Compensation of fibre impairments in digital coherent systems, in *Proc. 34th Europ. Conf. Opt. Commun.* (ECOC'08), Brussels, Belgium (2008), paper Mo3D1
108. B. Spinnler, Equalizer design and complexity for digital coherent receivers. *IEEE J. Sel. Top. Quantum Electron.* **16**(5), 1180–1192 (2010)
109. G. Clark, S. Parker, S. Mitra, A unified approach to time- and frequency-domain realization of FIR adaptive digital filters. *IEEE Trans. Acoust. Speech Signal Process.* **31**, 1073–1083 (1983)



110. S.J. Savory, G. Gavioli, R.I. Killey, P. Bayvel, Transmission of 42.8 Gbit/s polarization multiplexed NRZ-QPSK over 6400 km of standard fiber with no optical dispersion compensation, in *Opt. Fiber Commun. Conf. and Nat. Fiber Opt. Eng. Conf.* (OFC/NFOEC'07), Anaheim, CA, USA (2007), Techn. Digest, paper OTuA1
111. D. Godard, Self-recovering equalization and carrier tracking in two-dimensional data communication systems. *IEEE Trans. Commun.* **28**, 1867–1875 (1980)
112. I. Fatadin, D. Ives, S.J. Savory, Blind equalization and carrier phase recovery in a 16-QAM optical coherent system. *J. Lightwave Technol.* **27**(15), 3042–3049 (2009)
113. B. Widrow, Thinking about thinking: the discovery of the LMS algorithm. *IEEE Signal Process. Mag.* **22**, 100–106 (2005)
114. S.J. Savory, Digital filters for coherent optical receivers. *Opt. Express* **16**, 804–810 (2008)
115. A. Leven, N. Noriaki, U.V. Koc, Y.-K. Chen, Frequency estimation in intradyne reception. *IEEE Photonics Technol. Lett.* **19**(6), 366–368 (2007)
116. M. Kuschnerov, D. Van den Borne, K. Piyawanno, F.N. Hauske, C.R.S. Fludger, T. Duthel, T. Wuth, J.C. Geyer, C. Schulien, B. Spinnler, E.-D. Schmidt, B. Lankl, Joint-polarization carrier phase estimation for XPM-limited coherent polarization-multiplexed QPSK transmission with OOK-neighbors, in *Proc. 34th Europ. Conf. Opt. Commun.* (ECOC'08), Brussels, Belgium (2008), paper Mo4D2
117. J.D. Proakis, M. Salehi, *Digital Communications*, 5th edn. (McGraw Hill, Singapore, 2008). ISBN 978-0-07-295716-7
118. A.J. Viterbi, A.M. Viterbi, Nonlinear estimation of PSK-modulated carrier phase with application to burst digital transmission. *IEEE Trans. Inf. Theory* **29**, 543–551 (1983)
119. E. Ip, J. Kahn, Feedforward carrier recovery for coherent optical communications. *J. Lightwave Technol.* **25**(9), 2675–2692 (2007)
120. C. Laperle, A. Savchenko, C. Li, G. Mak, M. O'Sullivan, 5120 km RZ-DPSK transmission over G.652 fiber at 10 Gb/s with no optical dispersion compensation, in *Opt. Fiber Commun. Conf. and Nat. Fiber Opt. Eng. Conf.* (OFC/NFOEC'05), Anaheim, CA, USA (2005), Techn. Digest, paper PDP27
121. T. Kupfer, C. Schulien, Maximum likelihood sequence estimation at 10 Gb/s, from concept to implementation, in *18th Ann. Meeting IEEE Lasers & Electro-Optics Soc.* (LEOS'05), Sydney, Australia (2005), Techn. Digest, paper THU4
122. W. Kester, *Analog-Digital Conversion, Analog Devices* (2004), Chap. 2. Also available as *The Data Conversion Handbook* (Elsevier/Newnes, 2005), ISBN 0-7506-7841-0. Online: [www.analog.com/library/analogDialogue/archives/39-06/data\\_conversion\\_handbook.html](http://www.analog.com/library/analogDialogue/archives/39-06/data_conversion_handbook.html)
123. W. Kester, *Analog-Digital Conversion, Analog Devices* (2004), Chap. 3. Also available as *The Data Conversion Handbook* (Elsevier/Newnes, 2005), ISBN 0-7506-7841-0. Online: [www.analog.com/library/analogDialogue/archives/39-06/data\\_conversion\\_handbook.html](http://www.analog.com/library/analogDialogue/archives/39-06/data_conversion_handbook.html)
124. Standard for terminology and test methods for analog-to-digital converters, IEEE Std 1241-2000, 2001
125. R.H. Walden, Performance trends for analog-to-digital converters. *IEEE Commun. Mag.* **37**(2), 96–101 (1999)
126. W. Kester, Aperture time, aperture jitter, aperture delay time – removing the confusion, *Analog Devices*, Tutorial MT-07 (2009), online: [www.analog.com/static/imported-files/tutorials/MT-007.pdf](http://www.analog.com/static/imported-files/tutorials/MT-007.pdf)
127. Y. Achiam, A.M. Kaplan, M. Seimetz, Systems with higher order modulation, in *Fibre Optic Communication*, ed. by H. Venghaus, N. Grote (Springer, Berlin, 2012), Chap. 8
128. H.T. Quynhanh, A. Suzuki, M. Yoshida, T. Hirooka, M. Nakazawa, A  $\lambda/4$ -shifted distributed-feedback laser diode with a fiber ring cavity configuration having an OSNR of 85 dB and a linewidth of 7 kHz. *J. Lightwave Technol.* **20**(18), 1578–1580 (2008)
129. P. Dong, C. Xie, L. Chen, L.L. Buhl, Y.-K. Chen, 112-Gb/s monolithic PDM-QPSK modulator in silicon. *Opt. Express* **20**(26), 624–629 (2012)
130. C. Doerr, L. Chen, D. Vermeulen, T. Nielsen, S. Azemati, S. Stulz, G. McBrien, X.-M. Xu, B. Mikkelsen, M. Givhechi, C. Rasmussen, S.-Y. Park, Single-chip silicon photonics

- 100-Gb/s coherent transceiver, in *Opt. Fiber Commun. Conf. (OFC'14)*, San Francisco, CA, USA (2014), Techn. Digest, paper Th5C.1
131. Fujitsu introduces World's first DP-QPSK LN modulator for 100 Gbps optical networks (Sept. 2009), [www.fujitsu.com/jp/group/foc/en/resources/news/press-releases/2009/0914.html](http://www.fujitsu.com/jp/group/foc/en/resources/news/press-releases/2009/0914.html)
  132. S. Corzine, P. Evans, M. Kato, G. He, M. Fisher, M. Raburn, A. Dentai, I. Lyubomirsky, A. Nilsson, J. Rahn, R. Nagarajan, C. Tsai, J. Stewart, D. Christini, M. Missey, V. Lal, H. Dinh, A. Chen, J. Thomson, W. Williams, P. Chavarkar, S. Nguyen, D. Lambert, S. Agashe, J. Rossi, P. Liu, J. Webjorn, T. Butrie, M. Reffle, R. Schneider, M. Ziari, C. Joyner, S. Grubb, F. Kish, D. Welch, 10-Channel  $\times$  40 Gb/s per channel DQPSK monolithically integrated InP-based transmitter PIC, in *Opt. Fiber Commun. Conf. and Nat. Fiber Opt. Eng. Conf. (OFC/NFOEC'08)*, San Diego, CA, USA (2008), Techn. Digest, paper PDP18
  133. P. Schvan, A 22 GS/s 5-b ADC in 0.13  $\mu$ m SiGe BiCMOS, in *Proc. IEEE Internat. Solid-State Circ. Conf. (ISSCC'06)*, San Francisco, CA, USA (2006), pp. 572–573
  134. P. Schvan, D. Pollex, T. Bellingrath, A 22 GS/s 6b DAC with integrated digital ramp generator, in *Proc. IEEE Internat. Solid-State Circ. Conf. (ISSCC'05)*, San Francisco, CA, USA (2005), pp. 122–123
  135. M. Nagatani, H. Nosaka, S. Yamanaka, K. Sano, K. Murata, A 32-GS/s 6-bit double-sampling DAC in InP HBT technology, in *Proc. IEEE Compound Semicond. Integr. Circuits Symp.*, Greensboro, NC, USA (2009), [10.1109/csics.2009.5315628](https://doi.org/10.1109/csics.2009.5315628)
  136. S. Halder, H. Gustat, C. Scheytt, A. Thiede, A 20 GS/s 8-bit current steering DAC in 0.25  $\mu$ m SiGe BiCMOS technology, in *Proc. Eur. Microw. Integr. Circuits Conf.*, Amsterdam, The Netherlands (2008), pp. 147–150
  137. T. Ellermeyer, R. Schmid, A. Bielik, J. Rupeter, M. Möller, DA and AD converters in SiGe technology: speed and resolution for ultra high data rate applications, in *Proc. 36th Europ. Conf. Opt. Commun. (ECOC'10)*, Torino, Italy (2010), paper Th.10.A.6
  138. Y.M. Greshishchev, D. Pollex, S.-C. Wang, M. Besson, P. Flemeke, S. Szilagy, J. Aguirre, C. Falt, N. Ben-Hamida, R. Gibbins, P. Schvan, A 56 GS/s 6b DAC in 65 nm CMOS with  $256 \times 6b$  memory, in *Int. Solid-State Circ. Conf. (ISSCC'11)*, San Francisco, CA, USA (2011), pp. 194–196, Techn. Digest
  139. M. Nagatani, H. Nosaka, K. Sano, K. Murata, K. Kurishima, M. Ida, A 60-GS/s 6-bit DAC in 0.5  $\mu$ m InP HBT technology for optical communication systems, in *Proc. Comp. Semicond. Integr. Circ. Symp. (CSICS'11)*, Waikoloa, HI, USA (2011), Techn. Digest, paper G.3
  140. Fujitsu. Digital to analog converter. (Mar. 2012). [Online]. Available: [www.fujitsu.com/downloads/MICRO/fme/documentation/c60.pdf](http://www.fujitsu.com/downloads/MICRO/fme/documentation/c60.pdf)
  141. Tektronix. Tektronix announces world's fastest 10-bit commercial DAC. (Mar. 2013) <http://component-solutions.tek.com/news-library/Tektronix%20Component%20Solutions%20Announces%20Worlds%20Fastest%2010-bit%20Commercial%20DAC%20-%2020031813.pdf>
  142. K. Poulton, R. Neff, B. Setterberg, B. Wuppermann, T. Kopley, R. Jewett, J. Pernillo, C. Tan, A. Montijo, A 20 GS/s 8b ADC with a 1 MB memory in 0.18  $\mu$ m CMOS, in *Proc. Int. Solid-State Circuits Conf. (ISSCC'03)*, San Francisco, CA, USA (2003), pp. 318–319
  143. P. Schvan, D. Pollex, S.-C. Wang, C. Falt, N. Ben-Hamida, A 22 GS/s 5b ADC in 0.13  $\mu$ m SiGe BiCMOS, in *Proc. IEEE Internat. Solid-State Circ. Conf. (ISSCC'06)*, San Francisco, CA, USA (2006), pp. 572–573
  144. J. Lee, J. Weiner, P. Roux, A. Leven, Y.-K. Chen, A 24 GS/s 5-b ADC with closed-loop THA in 0.18  $\mu$ m SiGe BiCMOS, in *Proc. IEEE Custom Integr. Circ. Conf. (CICC'08)*, San Jose, CA, USA (2008), pp. 313–316
  145. P. Schvan, J. Bach, C. Falt, P. Flemke, R. Gibbins, Y. Greshishchev, N. Ben-Hamida, D. Pollex, J. Sitch, S.-C. Wang, J. Wolczanski, A 24 GS/s 6b ADC in 90 nm CMOS, in *Proc. IEEE Internat. Solid-State Circ. Conf. (ISSCC'08)*, San Francisco, CA, USA (2008), pp. 544–545
  146. I. Dedic, 56 GS/s ADC: enabling 100GbE, in *Opt. Fiber Commun. Conf. and Nat. Fiber Opt. Eng. Conf. (OFC/NFOEC'10)*, San Diego, CA, USA (2010), Techn. Digest, paper OThT6

147. Fujitsu, Factsheet LUKE-ES55 – 65 GSa/s 8 bit ADC. Online: [www.fujitsu.com/downloads/MICRO/fme/documentation/c63.pdf](http://www.fujitsu.com/downloads/MICRO/fme/documentation/c63.pdf)
148. Fujitsu, ROTTA 37-92 GSa/s 8-bit ADC family. Online: [www.fujitsu.com/cn/en/products/devices/semiconductor/fsp/asic/asic/ipmacro/networkingips/](http://www.fujitsu.com/cn/en/products/devices/semiconductor/fsp/asic/asic/ipmacro/networkingips/)

**Wilfried Idler** received the Diploma degree in Physics from University of Stuttgart in 1987. Between 1987 and 1996 he was at the Alcatel O/E components research division in Stuttgart, engaged in design and characterization of high speed DFB lasers, tunable lasers and wavelength converter structures and was involved in DFB laser technology transfers to Alcatel Optronics in France. Since 1996 he is with the Optical Networks Division of Alcatel and Alcatel-Lucent Bell Labs in Stuttgart. He was contributing to the world-wide first 40 Gb/s field trials and to various  $N \times 40$  Gb/s multi-Terabit transmission experiments and the related postdeadline papers at OFC and ECOC. Subsequently he was engaged at the 40 Gb/s and the 100 Gb/s product development of Alcatel-Lucent. His current research interest are coherent few carrier 1 Tb/s systems. Following his long standing experience on optical transmission systems, optical components and subsystems he was representing Alcatel-Lucent at the ITU-T study group 15 for a 10 years period. As expert on modulation formats and he was program committee member of OFC and regularly serves as referee for various journals. He published more than 100 journal and conference papers and holds numerous patent applications.

**Fred Buchali** received the diploma degree in electrical engineering in 1988 and the Ph.D. degree in 1991 from Humboldt-University Berlin. During his Ph.D. he worked on InGaAs/InP p–i–n photodiodes for fiber-optic communication. In 1991 he joined Duisburg University where he was involved in the research on InAlAs/InGaAs HFET and MSM-detectors. 1992 Fred Buchali joined Alcatel-Lucent Germany, where he was part of the optoelectronics components research department. There he worked on optimized pin photodiode processes for 10 Gb/s application. In 1999 he joined the optical transmission systems group, where he started research on optical and electrical impairment mitigation techniques at 10 and 40 Gb/s by analog electrical and optical techniques. During emerging coherent transmission technology he substantially contributed to the discovery of OFDM in optics. His current research interests cover coherent few carrier systems for 1 Tb/s and beyond using higher order modulation formats including the transmission aspects of the optical fiber and the digital signal processing. Fred Buchali was member of the OFC technical program committee and contributed continuously as reviewer for various journals. He published more than 100 journal and conference papers and holds more than 30 patent applications.